THE ASTROPHYSICAL JOURNAL SUPPLEMENT SERIES, 91:507–551, 1994 April

SURFACE PHOTOMETRY OF LOW-LUMINOSITY RADIO GALAXIES

LOURDES DE JUAN,[1] LUIS COLINA,[1,2] AND ISMAEL PÉREZ-FOURNON[3]
Received 1993 March 22; accepted 1993 September 10

ABSTRACT

We present the results on the optical morphology and structure of 25 low-luminosity radio galaxies. The radial dependence of parameters like the surface brightness, ellipticity, center, and position angle of the isophotes is presented to study the properties of the galaxies. Results for individual objects are discussed.

Subject headings: galaxies: photometry — galaxies: structure — radio continuum: galaxies

1. INTRODUCTION

In the past years, the extensive investigations on high-luminosity radio galaxies (Heckman et al. 1986; Hutchings 1987; Baum et al. 1988; Smith & Heckman 1989a) have led to a clearer understanding of this class of systems. They show a distorted optical morphology that has been interpreted as evidence of collisions or mergers between galaxies with a large gas content. There is also some evidence that these gravitational processes are able to generate a nonthermal activity in the nucleus of these galaxies.

On the contrary, studies of low-luminosity radio galaxies are very sparse. Some of them (Colina & Pérez-Fournon 1990a, b; Borne & Colina 1993; González-Serrano, Carballo, & Pérez-Fournon 1993) suggest that similar tidal interactions or merging processes between elliptical galaxies can trigger the radio activity at lower levels. However, gravitational interaction does not seem to be the only factor that controls the activity. Also, the gas content in the circumnuclear regions may play an important role (Borne & Colina 1993). It is still unclear which of these physical processes (gravitational interaction, presence of gas, dynamics of gas and stars) is the main parameter in the generation and maintenance of the nonthermal radio activity in low-luminosity radio galaxies.

A first step for solving this question is to analyze the stellar and gas properties of the host galaxy, in order to detect signatures of gravitational interactions or mergers. In a second step, we could relate these properties with the generation and maintenance of nonthermal activity in the core of the galaxy (Borne & Colina 1993).

With this purpose we have started an optical survey of 25 low-luminosity radio galaxies with well-defined radio jets. In the present paper we analyze their stellar component, optical morphology, using an isophote fitting algorithm. In a future paper, data on the gaseous component will be added to this study. A third paper will be devoted to the analysis and interpretation of the results presented in the first two papers.

This survey can be used as a complement to those of high-luminosity radio galaxies and can also be compared with normal elliptical galaxy surveys (Kormendy 1984; Lauer 1985; Bender, Döbrereiner, & Möllenhoff 1988; Franx, Illingworth, & Heckman 1989; Peletier et al. 1990; Sparks et al. 1991) in order to decide what structural characteristics define the radioactive ellipticals as a class.

In § 2 a brief discussion of the sample selection and observations is given. Section 3 contains the data reduction and the surface photometry algorithm used in the analysis, as well as the photometric calibration of our data. In § 4 the results on individual galaxies are presented.

2. THE DATA

2.1. *The Sample*

The sample consists of 25 low luminosity radio galaxies within the redshift range $0.01 \le z \le 0.08$, $\delta \ge -12$ °. The radio luminosity at 1.4 GHz corresponds to log $P_{1.4}^{\mathrm{total}}$ = 24.28 W Hz^{-1}, in the mean. These galaxies have been selected from the survey of Colina & Pérez-Fournon (1990a,b) consisting of 47 low luminosity radio galaxies from the Bridle & Perley (1984) list of galaxies with well defined jets (see Table 1). First column indicates the galaxy name from NGC, 3C, 4C, or B2 catalogs; second column gives the coordinates for 1950; third column is the redshift value form Bridle & Perley (1984) and fourth column represents the integrated optical apparent magnitude. References for both coordinates and magnitudes can be found in Colina & Pérez-Fournon (1990b).

This sample cannot be considered as complete, but the fact that all these galaxies present similar radio properties at the VLA scale is an indicator for the same physical process to operate in these objects.

2.2. *Observations*

All the galaxies but NGC 708 were observed at the Calar Alto Observatory using a RCA CCD camera attached to the 2.2 m telescope, giving a scale of 0$''$351 pixel^{-1} and a field size of 3$'$0 by 1$'$9. The filter used was the Gunn-Thuan r band filter (Thuan & Gunn 1976). NGC 708 was observed at the Roque de los Muchachos Observatory, using the Stockholm CCD Camera at the 2.5 m Nordic Optical Teleccope, which gives a scale of 0$''$2 pixel^{-1} and a field size of 1$'$7 by 1$'$7. In this case, an R filter (λ_{eff} = 6600 Å, FWHM = 1040 Å) was used.

The exposure time was 10 minutes for NGC 708 and 20 to 30 minutes for the rest of the sample. The seeing, measured from star profiles in the CCD frames, was on average 1$''$8

[1] Dpto. de Física Teórica, C-XI, Universidad Autónoma de Madrid, Cantoblanco, 28049 Madrid, Spain.
[2] Postal address: Space Telescope Science Institute, 3700 San Martin Drive, Baltimore, MD 21218.
[3] Instituto de Astrofísica de Canarias, La Laguna, Tenerife, Spain.

TABLE 1
THE SAMPLE

Object	Coordinate (1950)	z	m_v
NGC 315	0055+30	0.0167	12.50
NGC 326	0055+26	0.0472	13.00
3C 31	0104+32	0.0169	12.14
NGC 541	0123−01	0.0181	13.00
NGC 708	0149+35	0.0160	14.50
4C 35.03	0206+35	0.0373	13.00
NGC 1044	0238+08	0.0214	13.27
3C 75	0255+05	0.0241	13.16
3C 78	0305+03	0.0288	12.94
NGC 1265	0314+41	0.0255	12.50
4C 35.16A	0704+35	0.0780	15.50
4C 53.16	0712+53	0.0640	15.00
NGC 4789	1251+27	0.0270	13.30
NGC 4782/3	1252−12	0.0138	13.50
NGC 4869	1256+28	0.0235	14.90
NGC 5127	1321+31	0.0161	13.90
NGC 5490	1407+17	0.0163	13.40
NGC 5532	1414+11	0.0237	12.21
3C 402N	1940+50	0.0247	14.00
NGC 7052	2116+26	0.0164	14.00
3C 449	2229+39	0.0171	13.20
B2 2236+35	2236+35	0.0277	15.00
NGC 7626	2318+07	0.0112	12.80
3C 465	2335+26	0.0293	15.00
4C 47.63	2354+47	0.0460	15.00

(FWHM). Details on the observations and basic reduction procedure can be found in Colina & Pérez-Fournon (1990a).

3. REDUCTION AND ANALYSIS

3.1. *Basic Reduction*

The basic electronic and flat-fielding reductions were done as outlined in Colina & Pérez-Fournon (1990a). The sky background was obtained in each frame taking the median of the pixel values in small boxes ($3''.5 \times 3''.5$) near the corners of the CCD frame; the mean value of these independent measurements was taken as the sky value to be subtracted.

A Hubble constant $H_0 = 75$ km s^{-1} Mpc^{-1} will be used throughout this paper.

3.2. *Absolute Photometry*

Published aperture photometry (Sandage 1973; Longo & de Vaucouleurs 1983, 1985; Burnstein et al. 1987) has been used to calibrate the data. The magnitudes and colors have been K-corrected following Pence (1976) and corrected for Galactic extinction. Since most of these are *UBVR* data, we had to transform into r-magnitudes following Kent (1985):

$$r = B - 0.34 - 1.57(B - V) .$$

This procedure was found to be very effective: we have checked it by comparing our results against those published in other surveys (Franx et al. 1989; Smith & Heckman 1989b; Peletier et al. 1990; González-Serrano & Pérez-Fournon 1991; González-Serrano et al. 1993). The discrepancies between our r-magnitudes and their R-magnitudes have been evaluated with the relation given in Kent (1985), $r = R + 0.43 + 0.15$ $(B - V)$, and are of the order of $\Delta m = \pm 0.05$ mag.

For NGC 708 no absolute photometry was available. However, we have used the R brightness profile from Smith & Heckman (1989b) in the inner $2''$–$8''$ to rescale our profile in counts s^{-1}.

3.3. *Surface Photomery Algorithm*

We have used a numerical method based on the analysis of the intensity of the galaxy by elliptical fitting of its isophotes. This method is a version of the GASP package (Cawson 1983) improved by González-Serrano & Pérez-Fournon (Pérez-Fournon et al. 1988; González-Serrano 1989; González-Serrano & Pérez-Fournon 1989, 1991) and running within MIDAS. Similar methods have been extensively used by several groups (e.g., Jedrzejewski 1987; Smith & Heckman 1989a,b; Peletier et al. 1990).

The procedure to obtain the final results consists of several steps. First of all, a "mask-frame" covering all foreground objects is created. The fitting program ignores the masked objects and, for a given semi-major axis and estimated values of x-y center, position angle and ellipticity, samples the intensity around the trial ellipse at equal intervals in the eccentric anomaly θ. The intensity measurements are fitted by least-squares to

$$I = I_0\left[1 + \sum_{i=1}^{4} (A_i \sin i\theta + B_i \cos i\theta)\right] .$$

The amplitude of the coefficients A_1, B_1, A_2, and B_2 gives information about which ellipse parameters are wrong and by how much. These parameters are iteratively corrected until the amplitude of the corresponding harmonic has been reduced to zero. Then the semimajor axis length is increased by a factor and a new iteration begins.

The coefficients A_3, B_3, A_4, and B_4 are the shape parameters, B_4 being the most significant: box-shaped isophotes give $B_4 < 0$, perfect elliptical isophotes $B_4 = 0$, and pointed isophotes $B_4 > 0$.

This Fourier analysis gives the mean intensity I_0 (and therefore *luminosity profiles*), the ellipticity, position angle, and isophote center as a function of radius. This allows us to study the radial variations of these parameters.

After the fitting process ends, we construct a smooth galaxy model, interpolating between the intensities of the ellipses by means of a de Vaucouleurs law. The subtraction of this model from the original image allows us to remove the elliptical component and detect underlying structures (like disks, dust, optical counterparts of radio jets, etc.), if any.

When the analyzed object is a pair (or a group) of galaxies, the procedure is applied to the galaxies of the pair (group) in an iterative way. The initial mask-frame has to be constructed masking the main part of the companion galaxy, and part of the region between the two galaxies where the contribution of the companion is significant. The algorithm is then applied to the first galaxy, a first model is constructed, and subtracted to the original image. The residual image containing the light of the second galaxy is used as input for the fitting program to obtain a first model for the second galaxy, which is then subtracted to the original image. This new residual image contains the light of the first galaxy and it is used as the input to obtain the improved second model to the first galaxy. The process goes on, improving both models in each step, until the addition of the two models gives a resulting model that matches the system light distribution.

Lauer (1986) introduced an algorithm that fits simultaneously the intensity distribution of the objects in a group, but a drawback of his procedure was to consider concentric isophotes. Since this is not the case in our systems (e.g., see NGC 4782/3 and others below) and we are interested in measuring isophotes displacements, we have preferred to use the iterative decomposition algorithm better than Lauer's method.

A validation of this iterative decomposition procedure is given in the Appendix.

3.4. *Isophote Fitting Parameters*

The isophote fitting procedure has been applied to all the radio galaxies in the sample and also to the companions in the case of two or more galaxies sharing a common envelope or showing signs of isophotal distortions.

Contour plots of original and model images are given in Figure 1. Some of the models plotted have odd bumps (e.g., 3C 449) that appear at small scales (1″–2″), but this arises as a consequence of the removal of bright foreground stars before applying the isophote fitting algorithm.

We present in Figure 2 the resulting parameters of the isophote analysis. We have plotted the following parameters: (1) surface brightness, in magnitudes arcsec^{-2} versus radius, r ($r = \sqrt{ab}$, where a and b are the semi-major and semi-minor axis), and versus $r^{1/4}$; (2) Ellipticity, ϵ; (3) Position angle (in degrees) of the major axis; (4) Isophote centers, X_0, Y_0: their position expressed in pixels; (5) Fourier coefficient, B_4, of the term cos 4θ.

In these plots, the mark "80%" indicates the radius at which the available information corresponds only to 80%, or less, of the whole ellipse (the rest of the ellipse was masked or outside the CCD frame). We have marked this radius since it is difficult for the fitting program to find a stable and valid solution for the center of the isophote. This, together with the low signal-to-noise ratio at large distances, causes the artificial results observed in several plots of Figure 2, in the sense that isophote centers tend to wander away. The simulations presented in Appendix show that at radius $r \geq r_{80\%}$, deviations of the order of ~3 pixels may appear. Therefore, we can consider that, on average, the isophote displacements observed at $r \geq r_{80\%}$ with $\sqrt{\Delta X^2 + \Delta Y^2} \geq 3$ pixels are not reliable. The mark "sky" indicates the sky background level in each frame. Small circles in brightness profiles represent the point spread function of a star in the CCD frame. Error bars are only plotted when significant.

The parameters mentioned above are tabulated in Table 2. The sample of Table 2 shown here lists parameters for NGC 315. Table 2 is published in its entirety in computer-readable form on the AAS CD-ROM Series, Volume 2.

4. COMMENTS ON PECULIAR SOURCES

NGC 326.—This galaxy is a member of the Zwicky cluster 0056.9+2636. It appears as a dumbbell galaxy with two equally bright nuclei. There is also a smaller companion located in direction P.A. 201° of the system. The radio emission shows twin jets along direction P.A. 135° (Ekers et al. 1981).

Both galaxies show features not seen in normal ellipticals:

1. Strong isophote twist: NGC 326N shows a P.A. change of ΔP.A. ~ 90° between r = 3″–20″, while the south component has a minimum at r ~ 10″, with ΔP.A. ~ 40°.

2. Nonconcentric isophotes: Both galaxies show strong off-centering of their isophotes. Their values Δr correspond to 1″.8 and 2″.9 for NGC 326N and NGC 326S, respectively. The isophote centers of the north component are displaced to the NE, while those of the south one are displaced to the SW.

3C 31.—This galaxy is the brightest member of a chain (Arp 331) comprising several galaxies, which belong to the Zwicky cluster 0107.5+3212. It has an elliptical companion (NGC 382) at 33″ to the SW. Smith & Heckman (1989b) give V-magnitude, ellipticity, and position angle profiles for the main component of the system, and their results are in good agreement with ours.

The radio structure consists of two strong radio jets emerging from the nucleus of the main galaxy (NGC 383) in P.A. 341° and 160° (Butcher, van Breugel, & Miley 1980).

The parameters obtained for NGC 383 show discontinuities at radius r ~ 3″–3″.5 due to the presence of a dust ring. We have detected this ring in our residual image. However, we did not find the reported optical counterpart of the northern radio jet (Butcher et al. 1980).

We find the following features in NGC 383:

1. Slight twist of its isophotes. The change in P.A. is slightly higher than typical in ellipticals, varying from 132° to 150°, between r ~ 30″ and r ~ 45″ and decreasing beyond this point.

2. Shifts of the isophote centers. The value Δr increases 1″.2 between r ~ 20″–30″, and decreases 0″.9 in the same region where the P.A. twists.

NGC 541.—This is an elliptical galaxy located in the cluster Abell 194. It is associated with PKS 0123−016A, a small head-tail radio source (van Breugel et al. 1985) near the larger and more powerful radio galaxy 3C 40 (PKS 0123−016B), which is associated with the nearby dumbbell system NGC 545/547.

The parameters are described below:

1. Large gradients in ellipticity. This galaxy shows rounder isophotes in the inner 10″ and an increase of $\Delta\epsilon$ ~ 0.2 between 10″ and 20″.

2. Nonconcentric isophotes. The isophote centers keep constant until r ~ 14″, moving then to the SW, being the outer isophotes (e.g., at r ~ 45″) displaced ~3″.7.

NGC 708.—This galaxy, located in the Abell cluster A262, has a dust lane almost perpendicular to the direction of its radio emission (Ebtener & Balick 1985), which extends along direction P.A. 70° (Parma et al. 1986).

Smith & Heckman (1989b) presented R-magnitude, ellipticity, and position angle profiles of this object. Their results agree with ours.

The resulting parameters show distortions in the inner ~2″ due to the presence of the dust lane. Ellipticity shows large gradients, varying form 0.03 at r ~ 8″ to 0.4 at r ~ 40″. Isophotes centers tends to move to the NW, being the outer isophotes (at r ~ 40″) displaced 1″.4 from the center.

4C 35.03.—This radio galaxy, located in the Zwicky cluster 0216.0+3625, consists of a two-sided jet along the NW-SE direction (Parma et al. 1987). At optical wavelengths, it shows a smaller companion located at 43″ in position P.A. 108°. At ~2″ from the center of the main galaxy there is a secondary source, but the resolution of the image (FWHM = 1″.89) did not allow us to analyze both nuclei individually. Therefore,

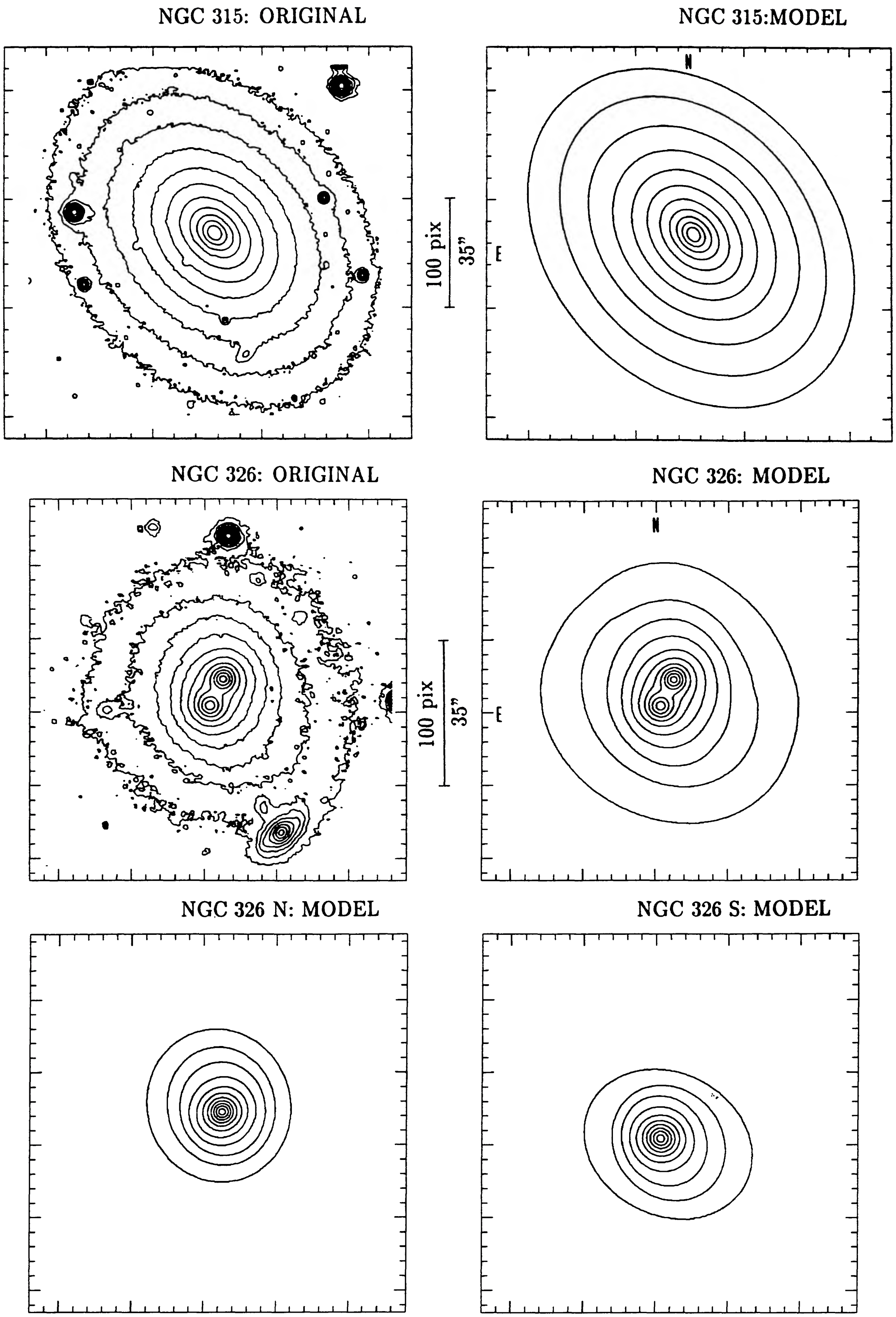

FIG. 1.—Contour map of original images and the obtained models. Contours are in half-magnitude steps; the outermost contour is at 23.5 mag arcsec^{-2} in NGC 541, NGC 1265, NGC 5127 and B2 2236+35; at 22.8 mag arcsec^{-2} in NGC 315, NGC 4789, and NGC 7052; at 23.0 mag arcsec^{-2} in 3C 31 and NGC 5490; at 23.3 mag arcsec^{-2} in NGC 326 and NGC 1044; at 23.6 mag arcsec^{-2} in 3C 78 and 4C 35.16; at 22.5 mag arcsec^{-2} in NGC 5532 and 3C 402 N; at 22.1 mag arcsec^{-2} in NGC 708; at 22.8 mag arcsec^{-2} in 4C 35.03; at 23.1 mag arcsec^{-2} in 3C 75; at 24.0 mag arcsec^{-2} in 4C 53.16; at 22.3 mag arcsec^{-2} in NGC 4782/4783; at 24.3 mag arcsec^{-2} in NGC 4869; at 23.2 mag arcsec^{-2} in 3C 449; at 23.3 mag arcsec^{-2} in 3C 465; at 22.3 mag arcsec^{-2} in NGC 7626; and at 24.2 mag arcsec^{-2} in 4C 47.63.

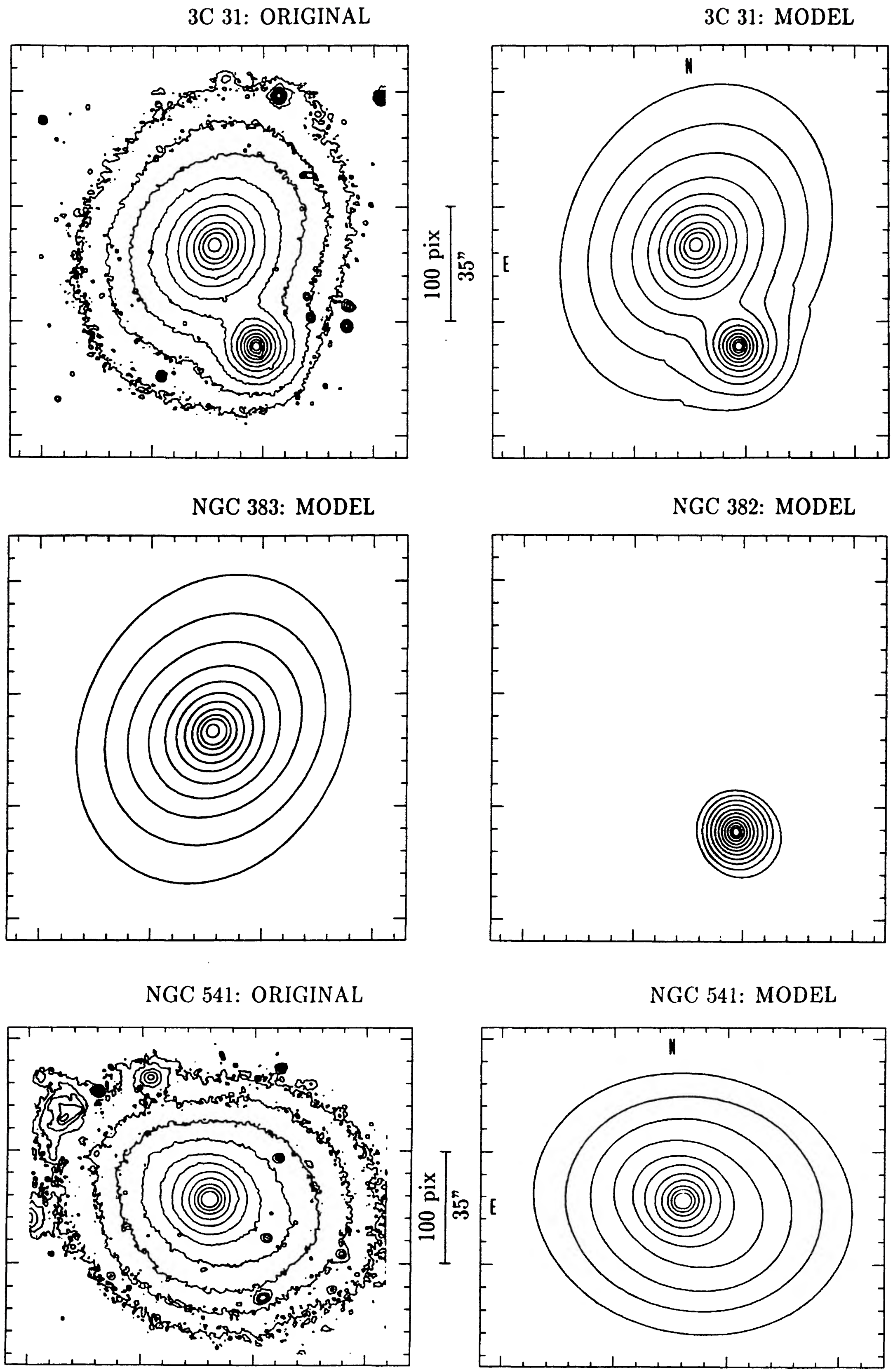

FIG. 1—*Continued*

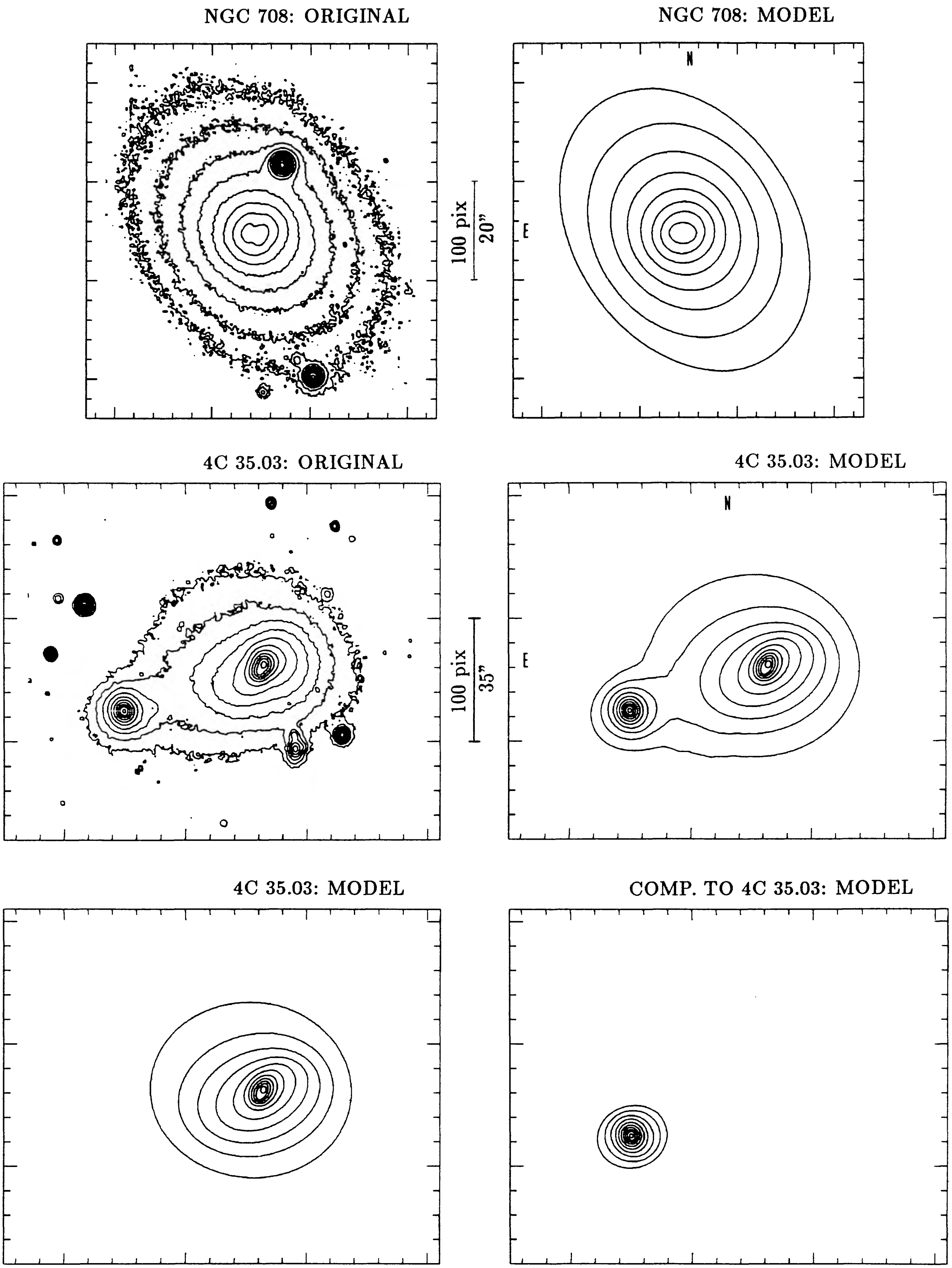

FIG. 1—*Continued*

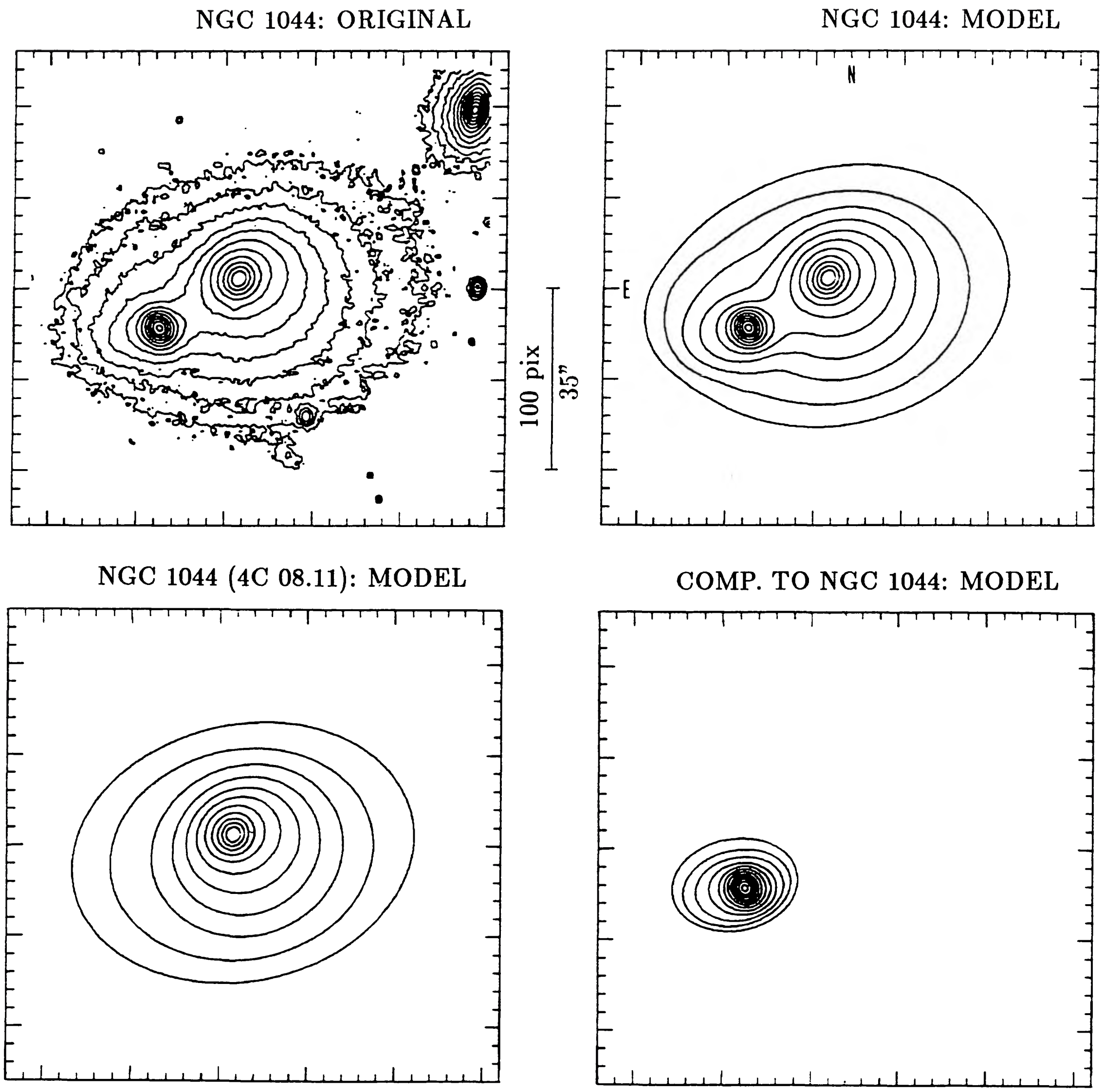

FIG. 1—*Continued*

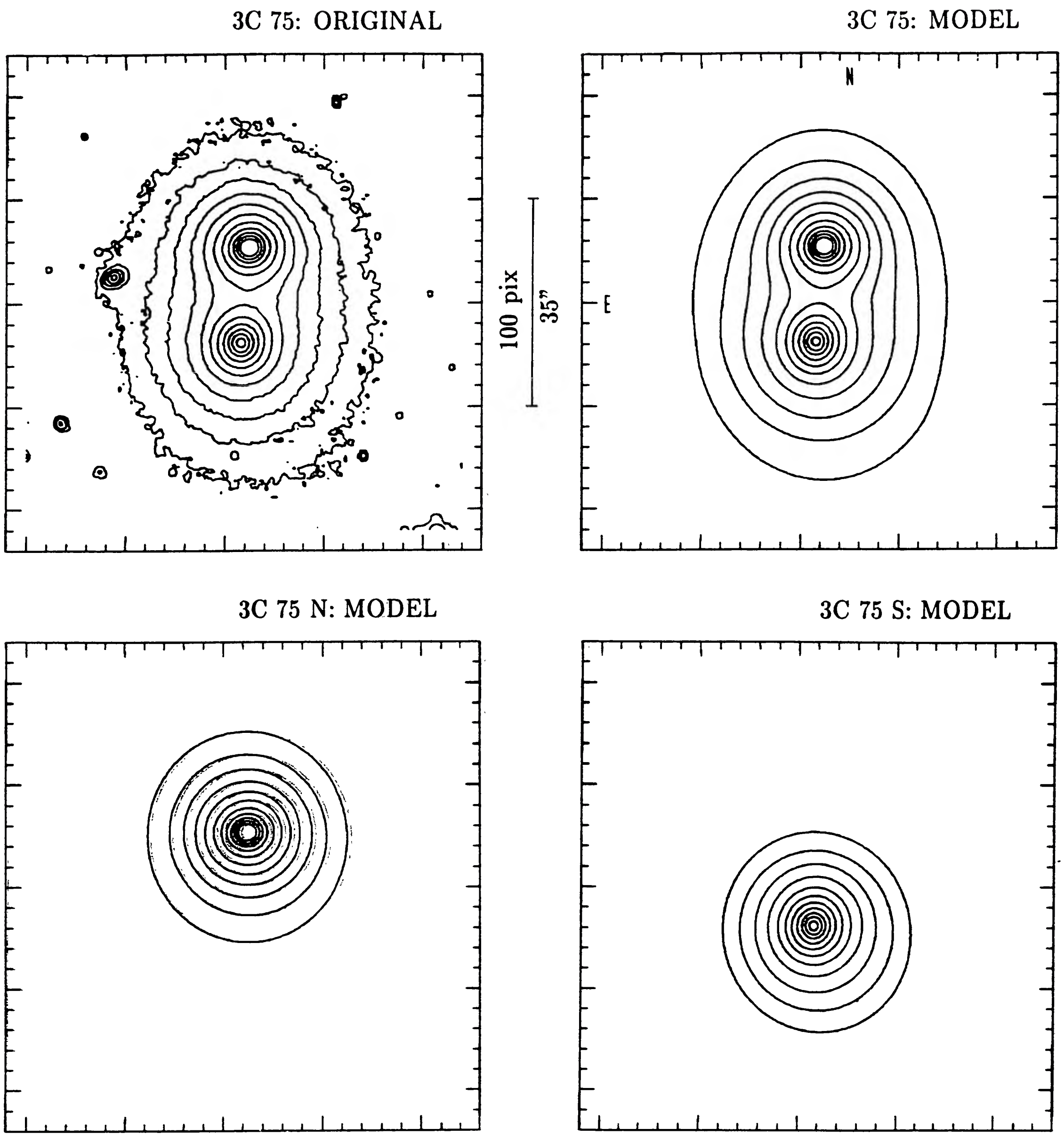

FIG. 1—*Continued*

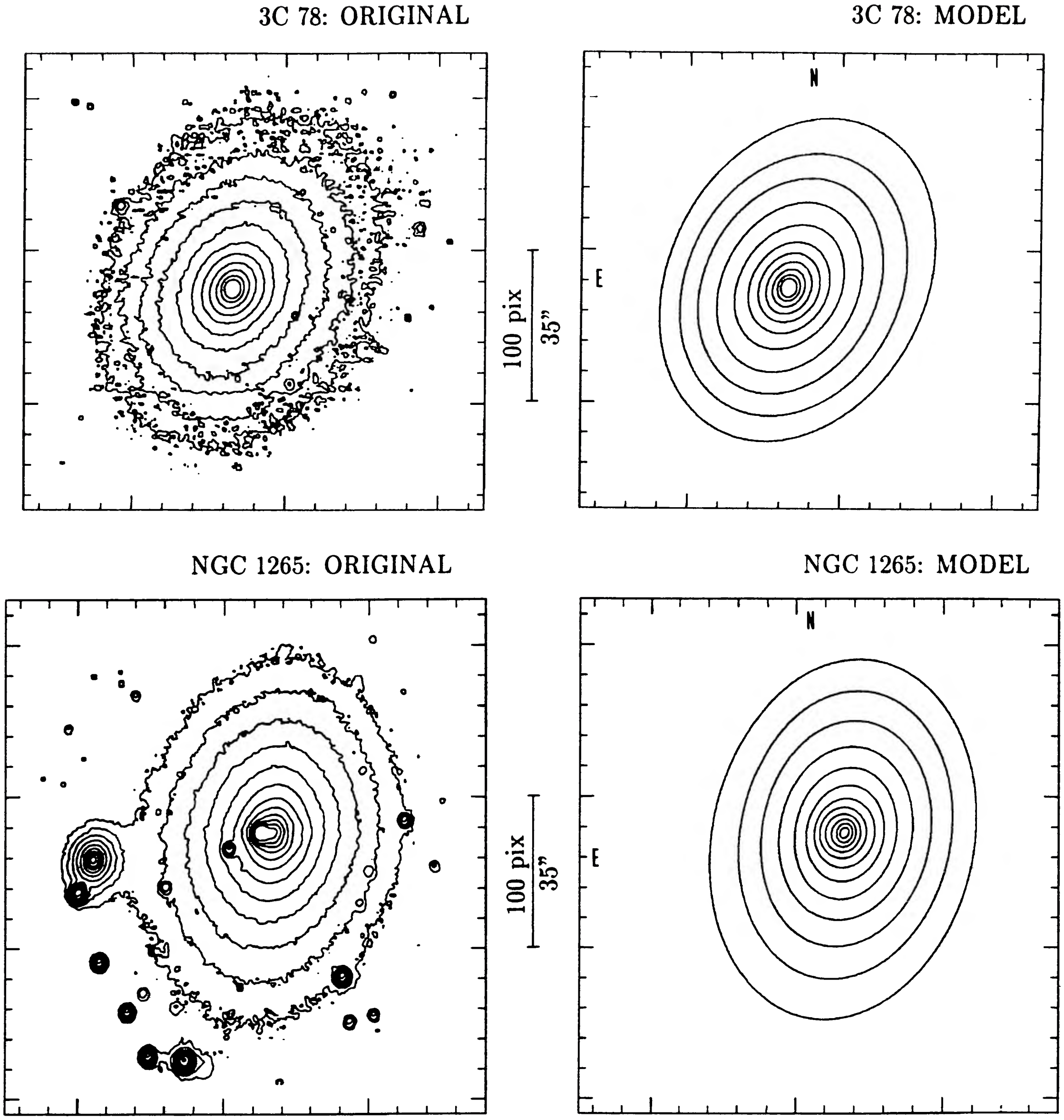

FIG. 1—*Continued*

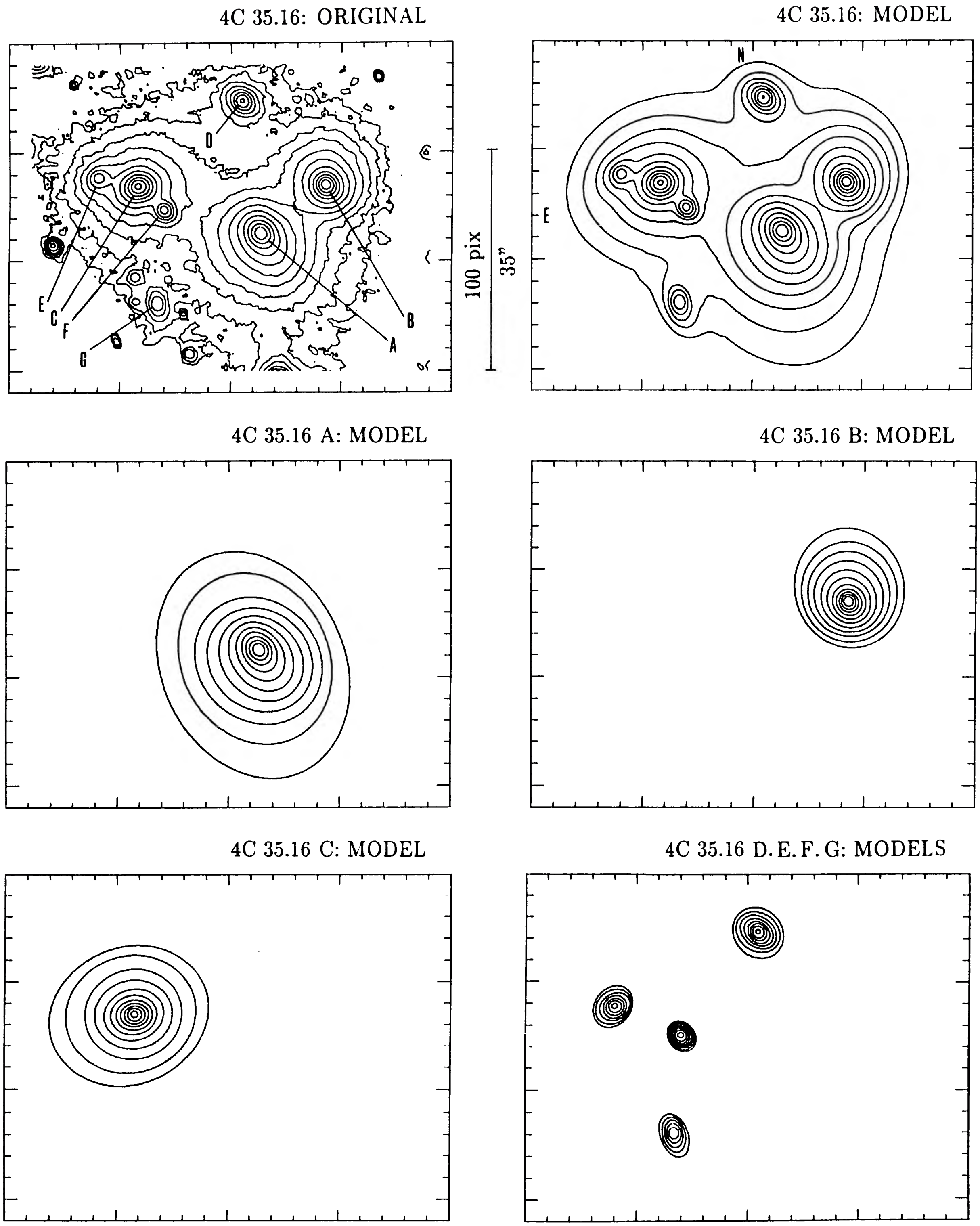

FIG. 1—*Continued*

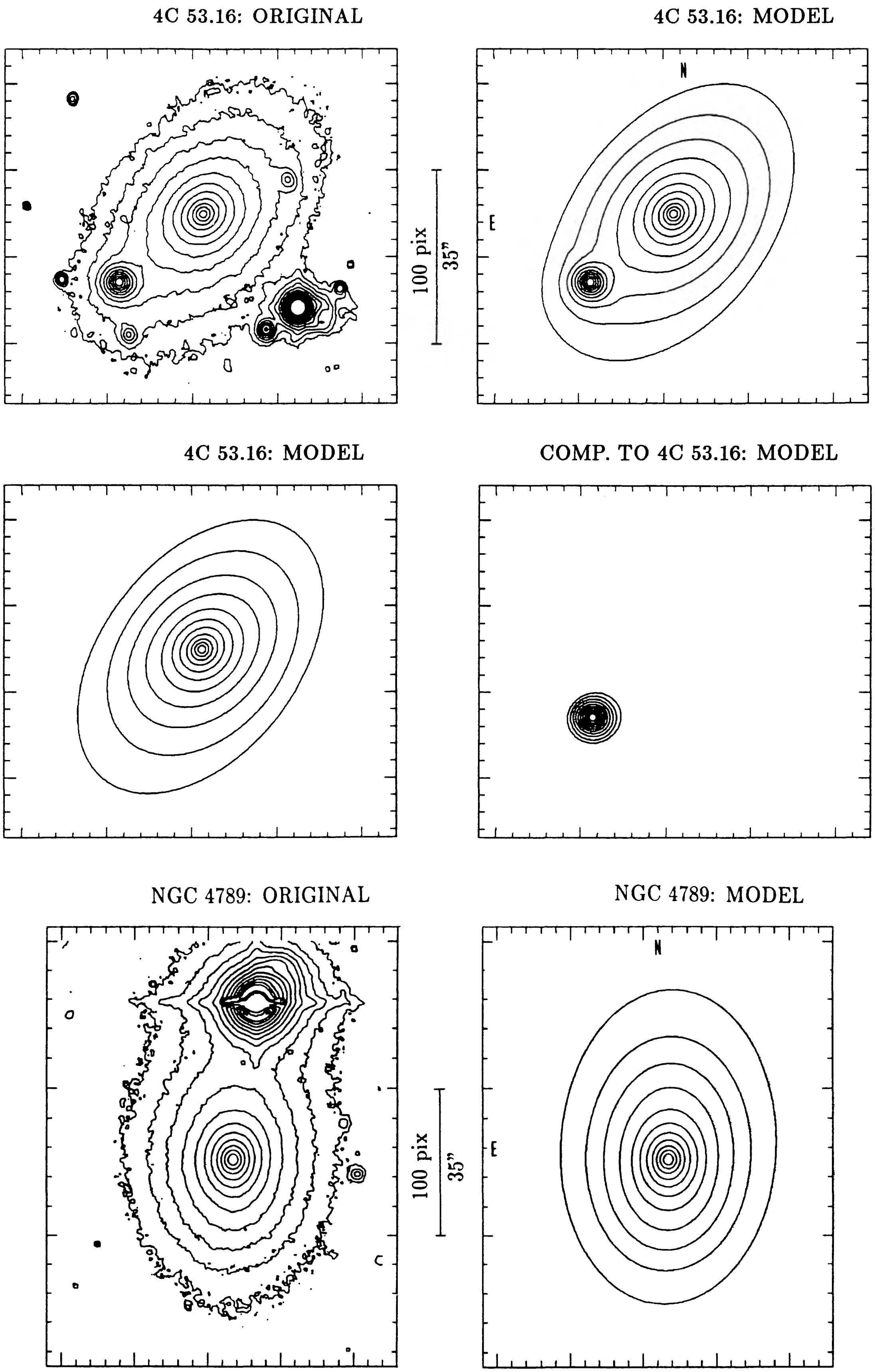

FIG. 1—*Continued*

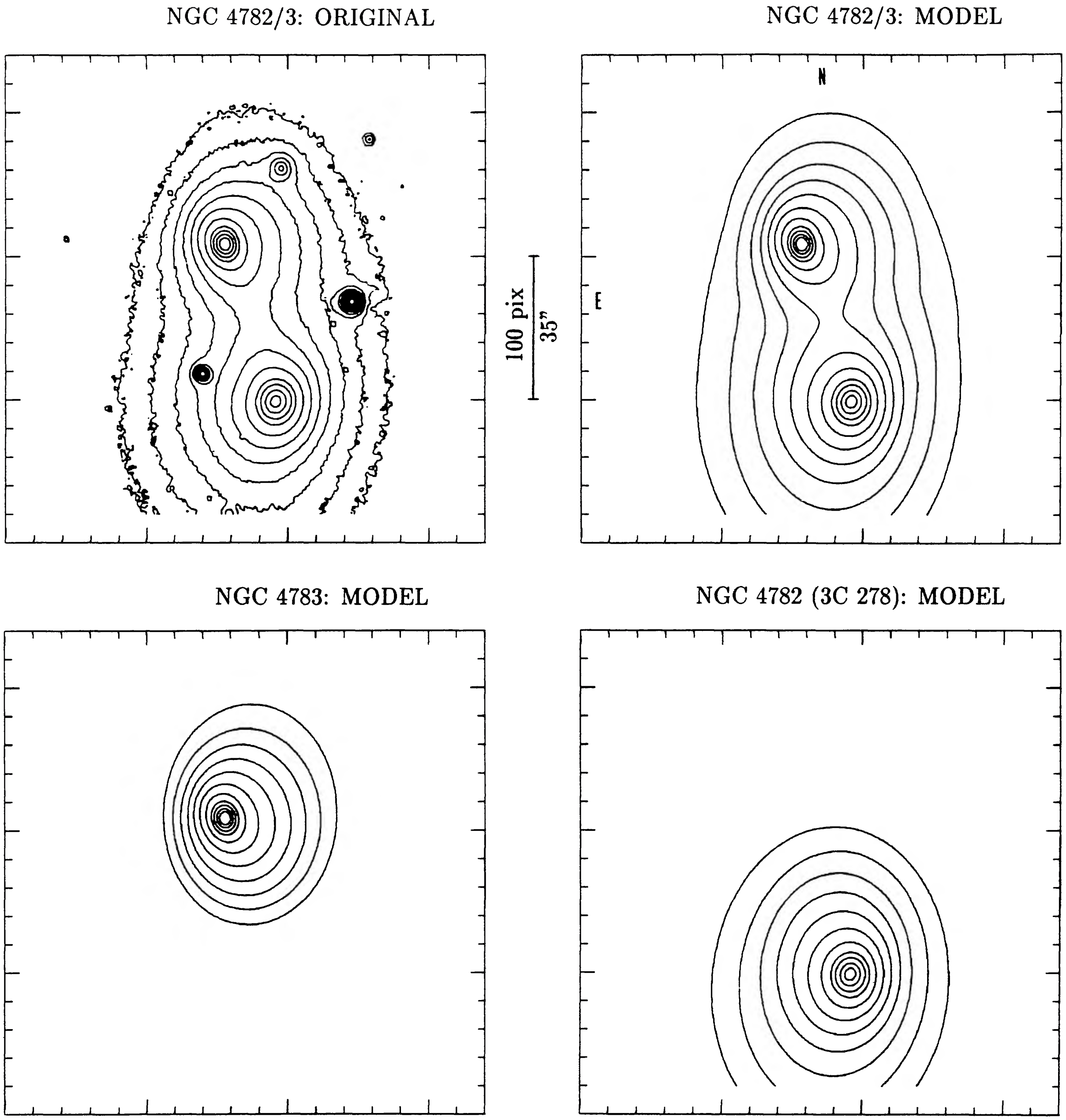

FIG. 1—*Continued*

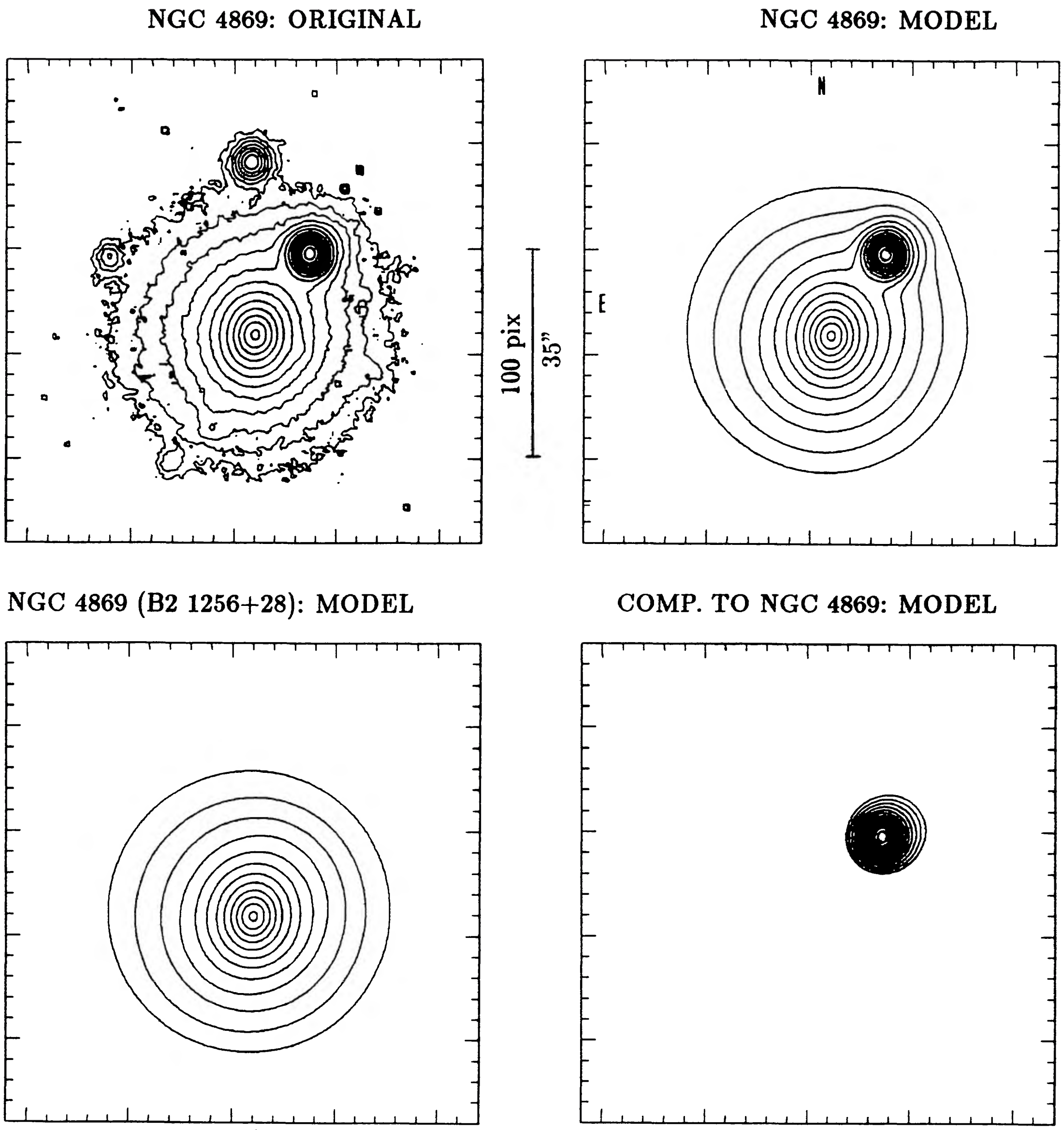

FIG. 1—*Continued*

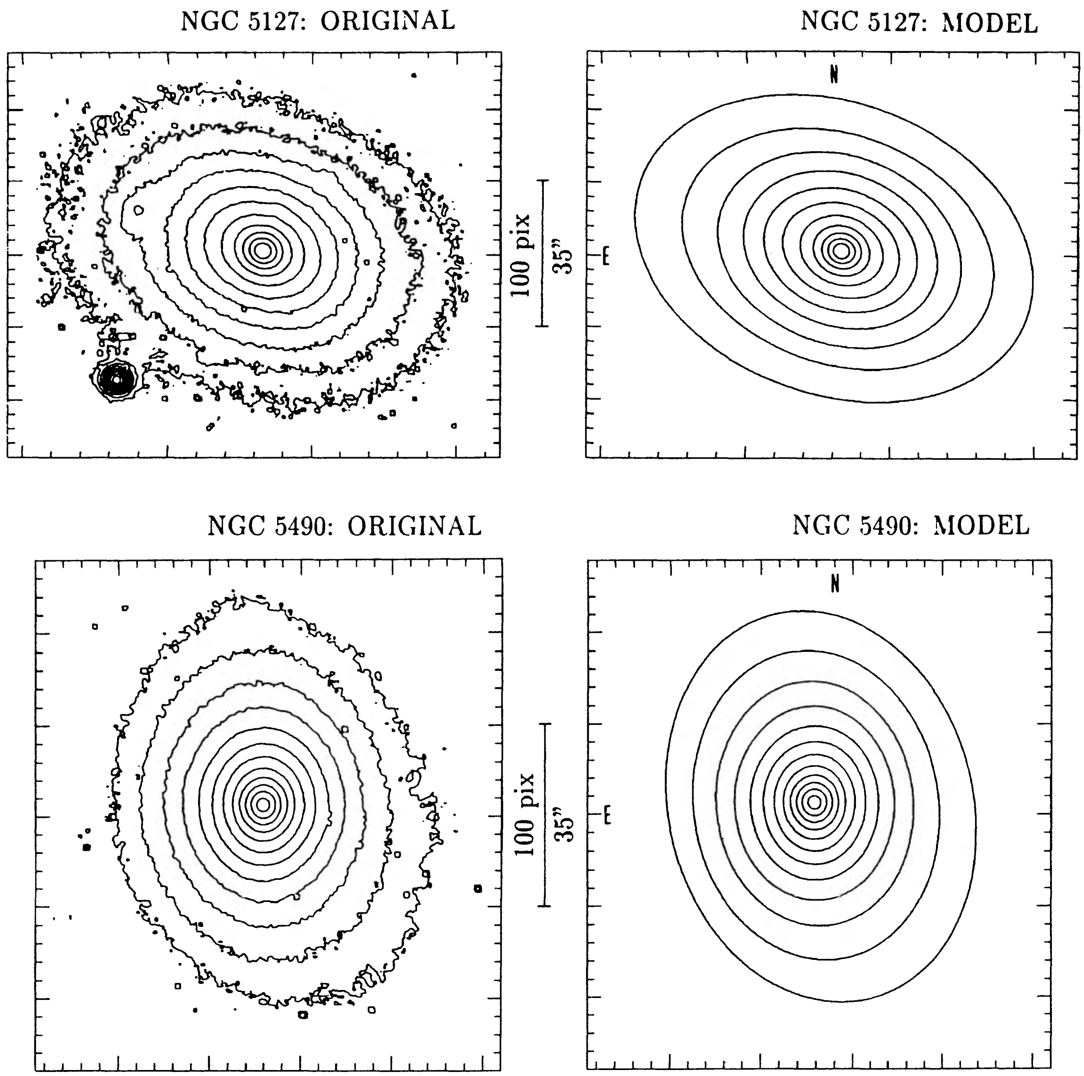

FIG. 1—*Continued*

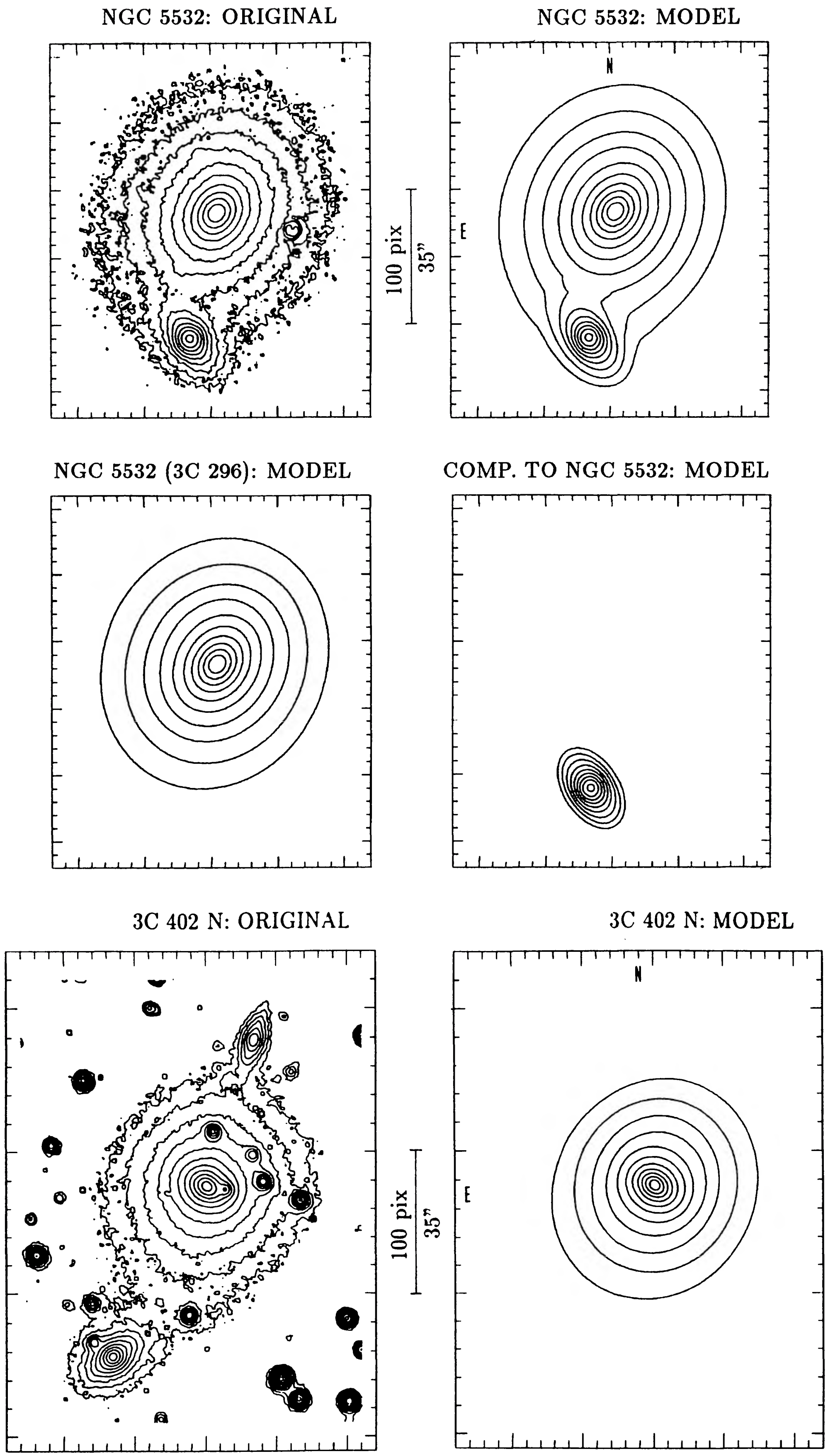

FIG. 1—*Continued*

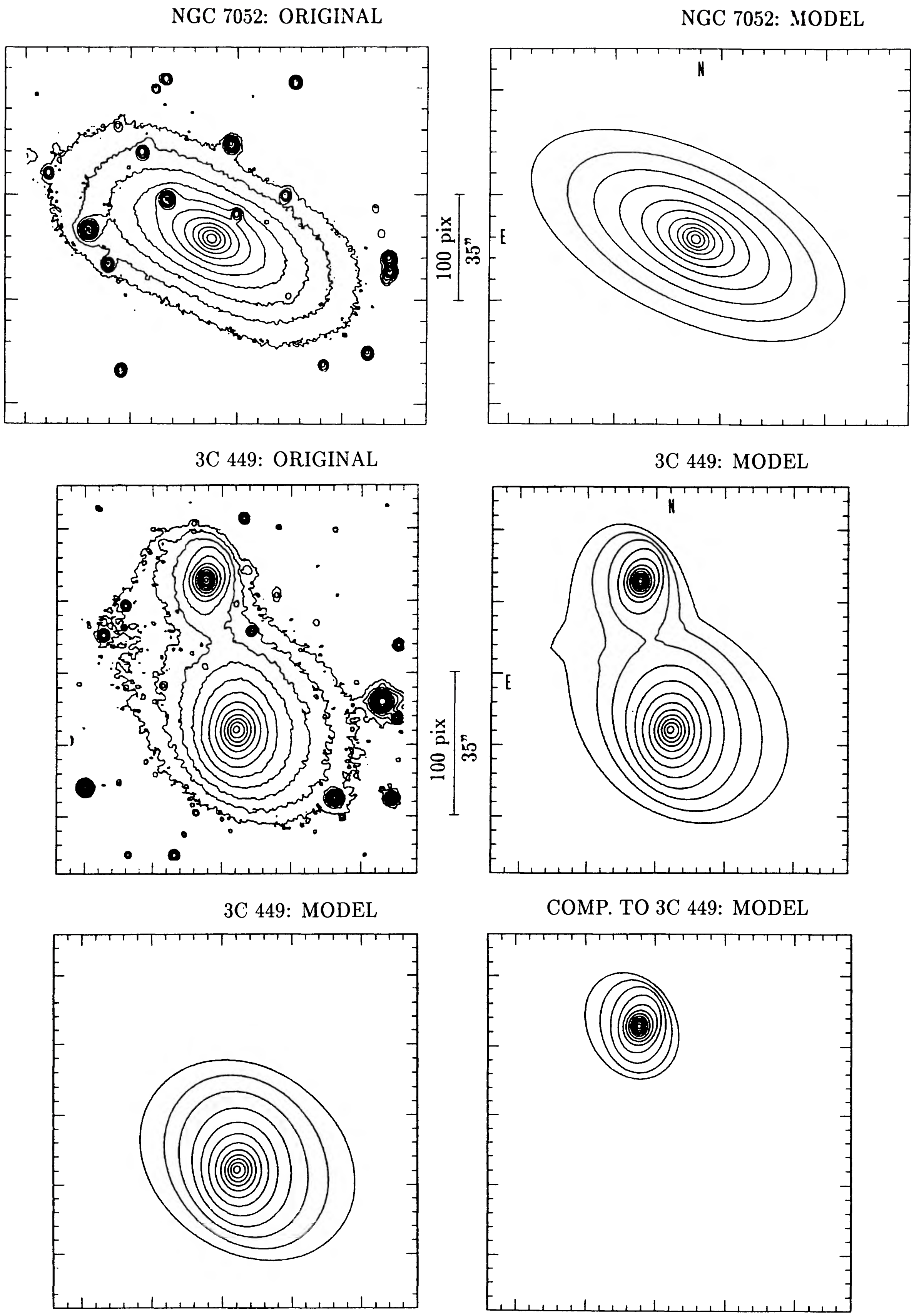

FIG. 1—*Continued*

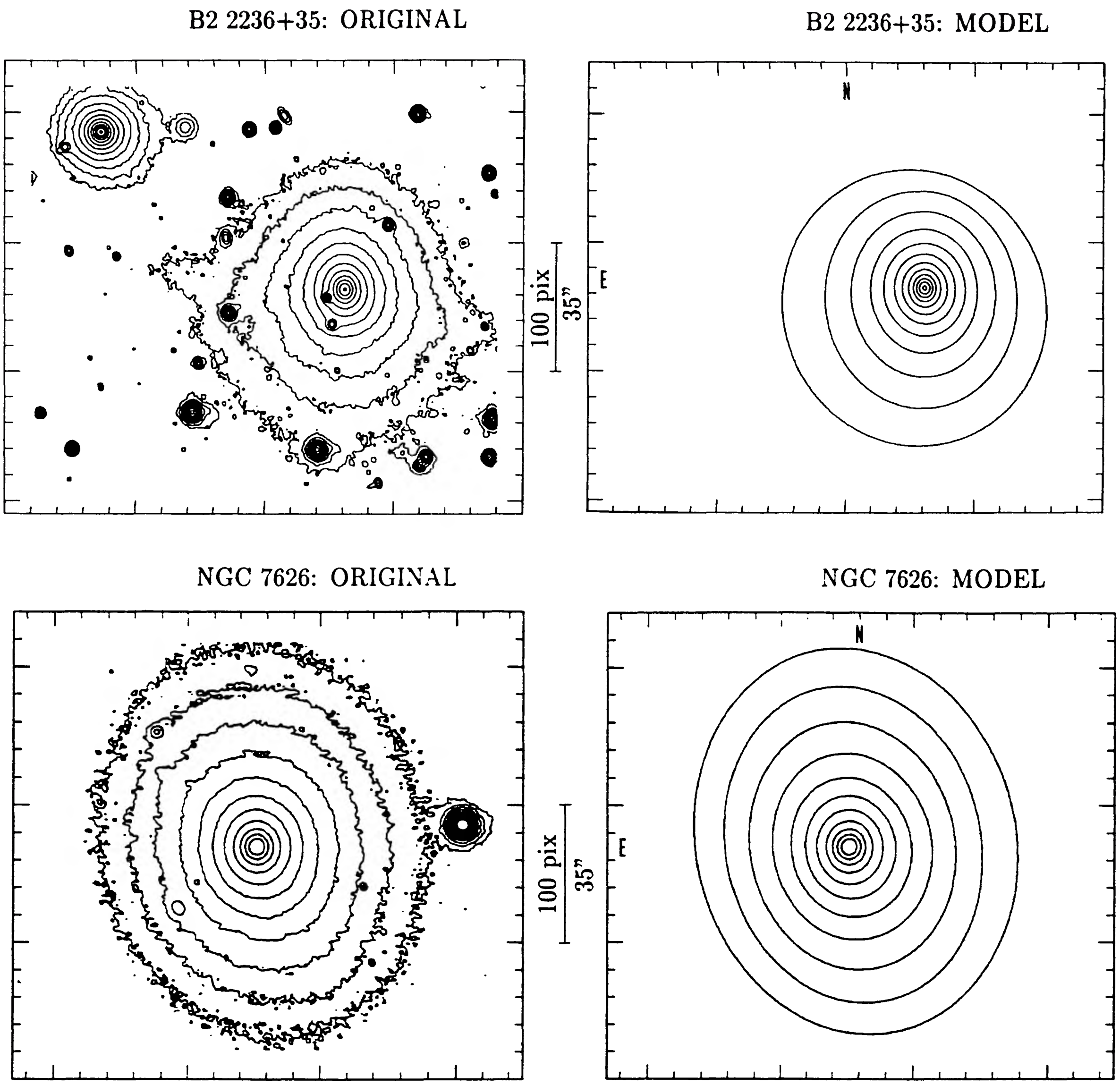

FIG. 1—*Continued*

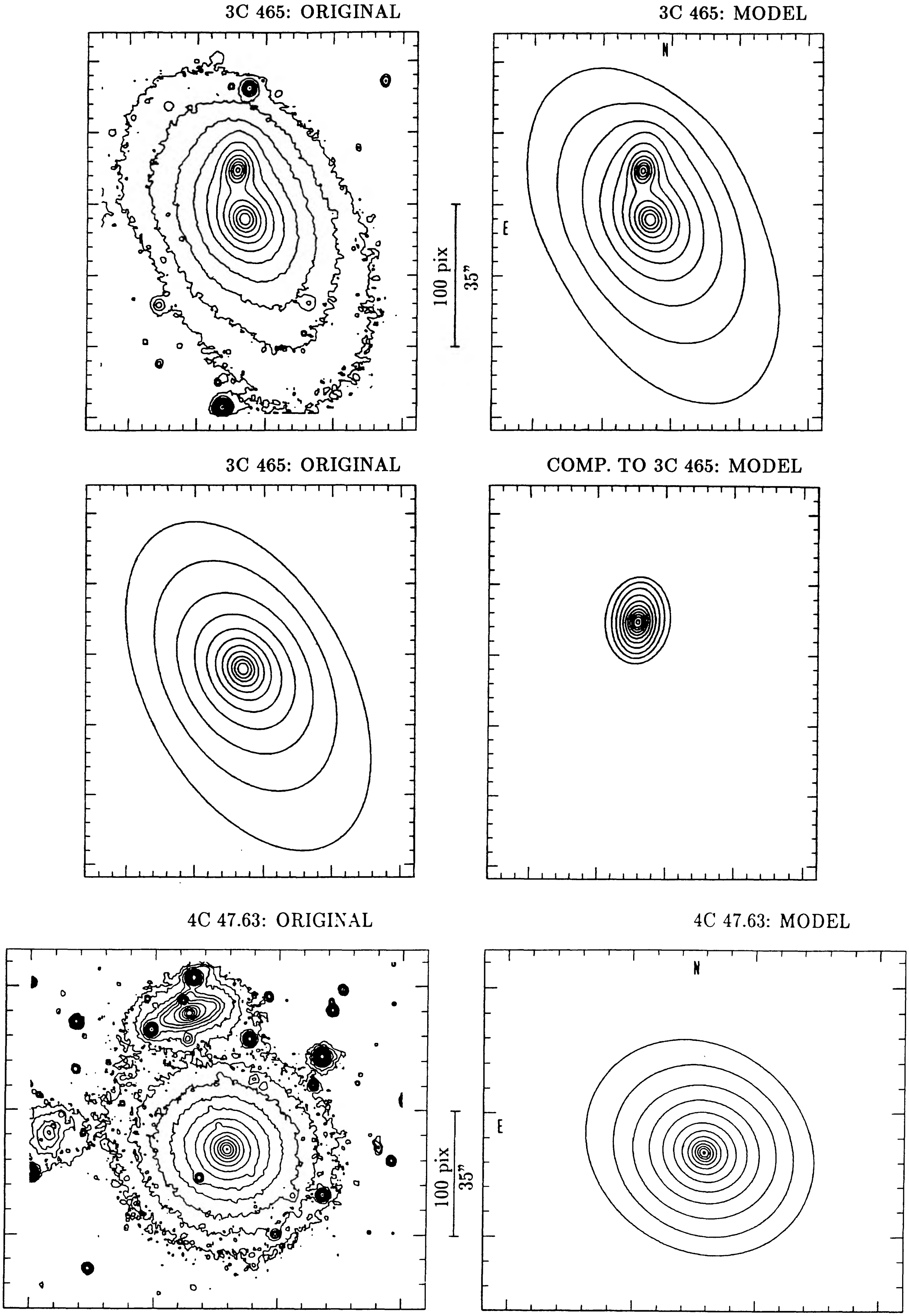

FIG. 1—*Continued*

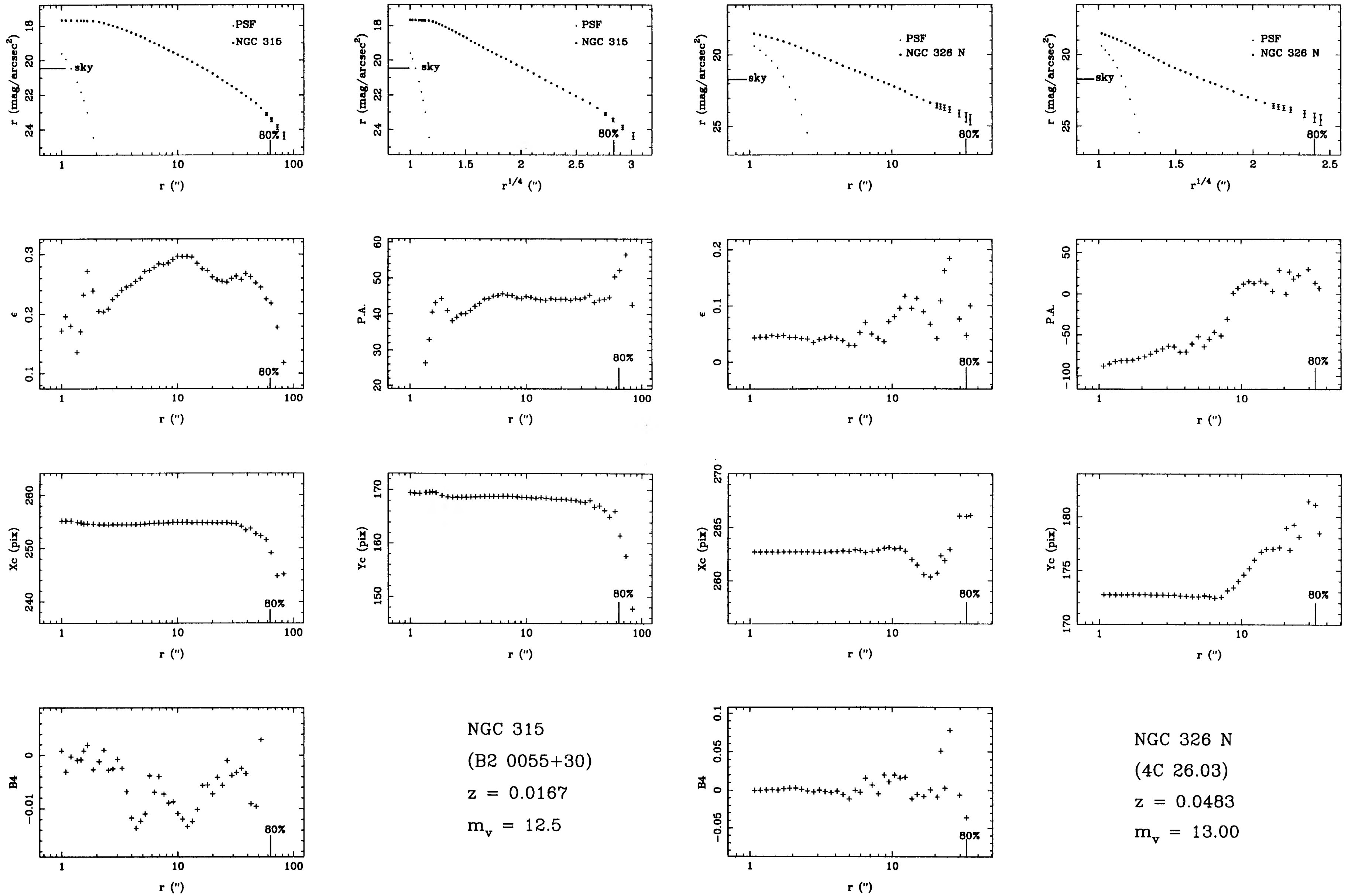

FIG. 2.—r band surface brightness profile, ellipticity, major-axis position angle, isophote center and B_4 as a function of radius are presented for each galaxy of the sample. The mark "80%" indicates the radius at which the fitting program found only 80% of the whole ellipse to fit (the rest of the ellipse was masked or out of the frame). The mark "sky" indicates the sky level. Small circles in brightness profiles represent the point spread function of a star. Error bars are only plotted when significant. Results of NGC 1265 must be carefully taken. There is a bright star near the nucleus of NGC 1265 which had to be masked for the fit. Although there is a mark of 80% at $r = 40''$, the valid fraction of ellipse is less tan 80% when $1'' < r < 4''.5$.

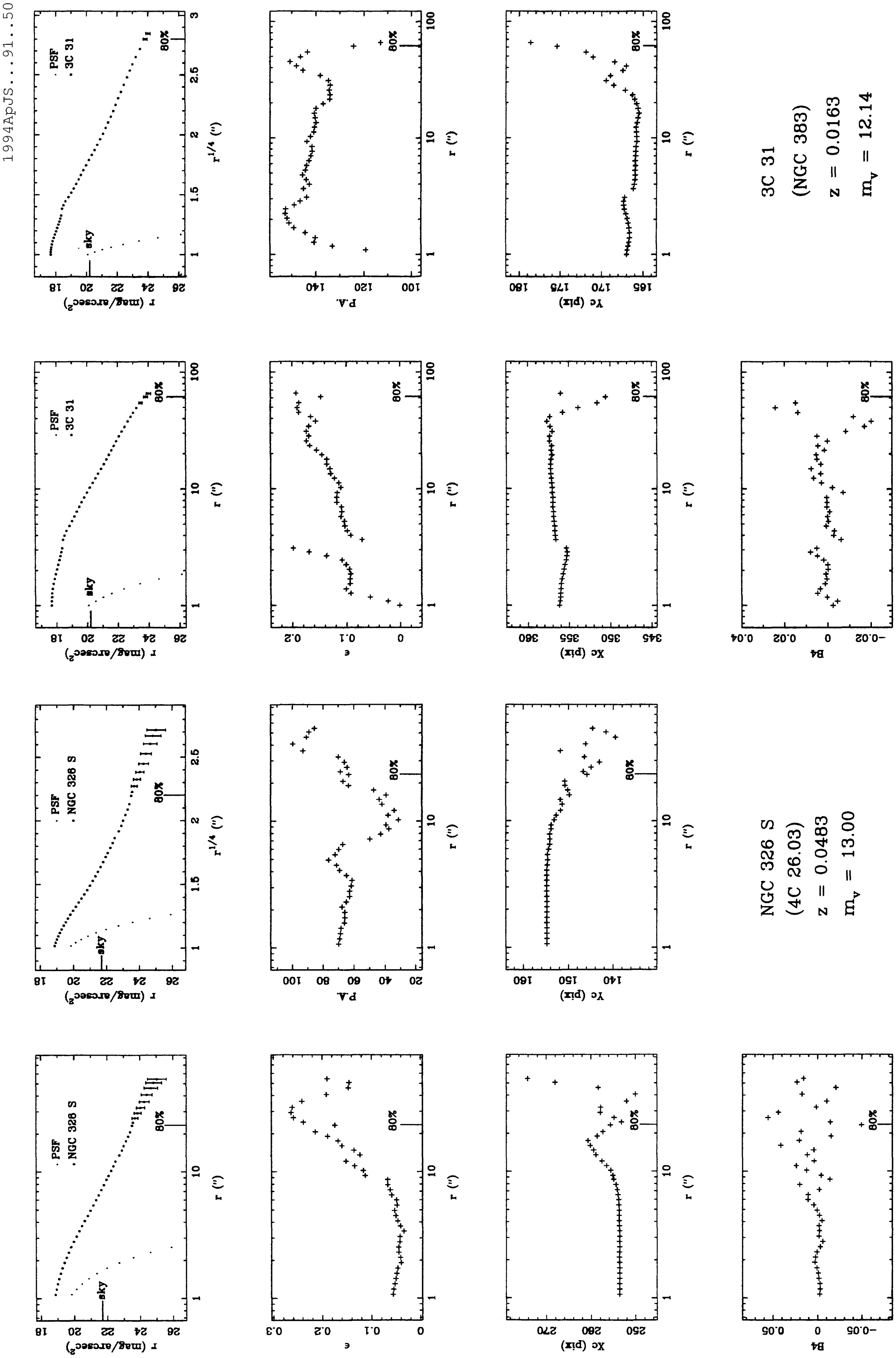

FIG. 2—*Continued*

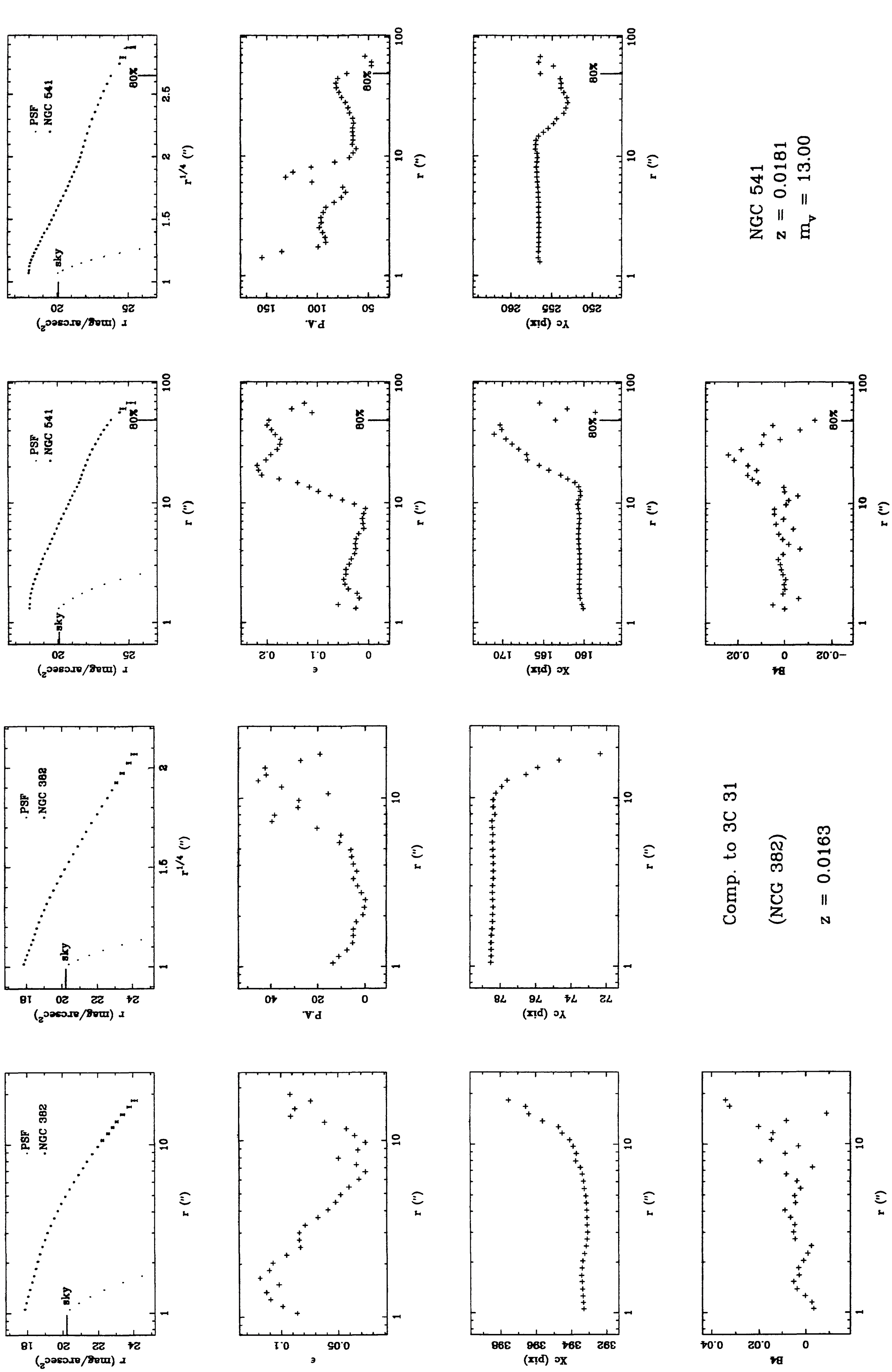

FIG. 2—*Continued*

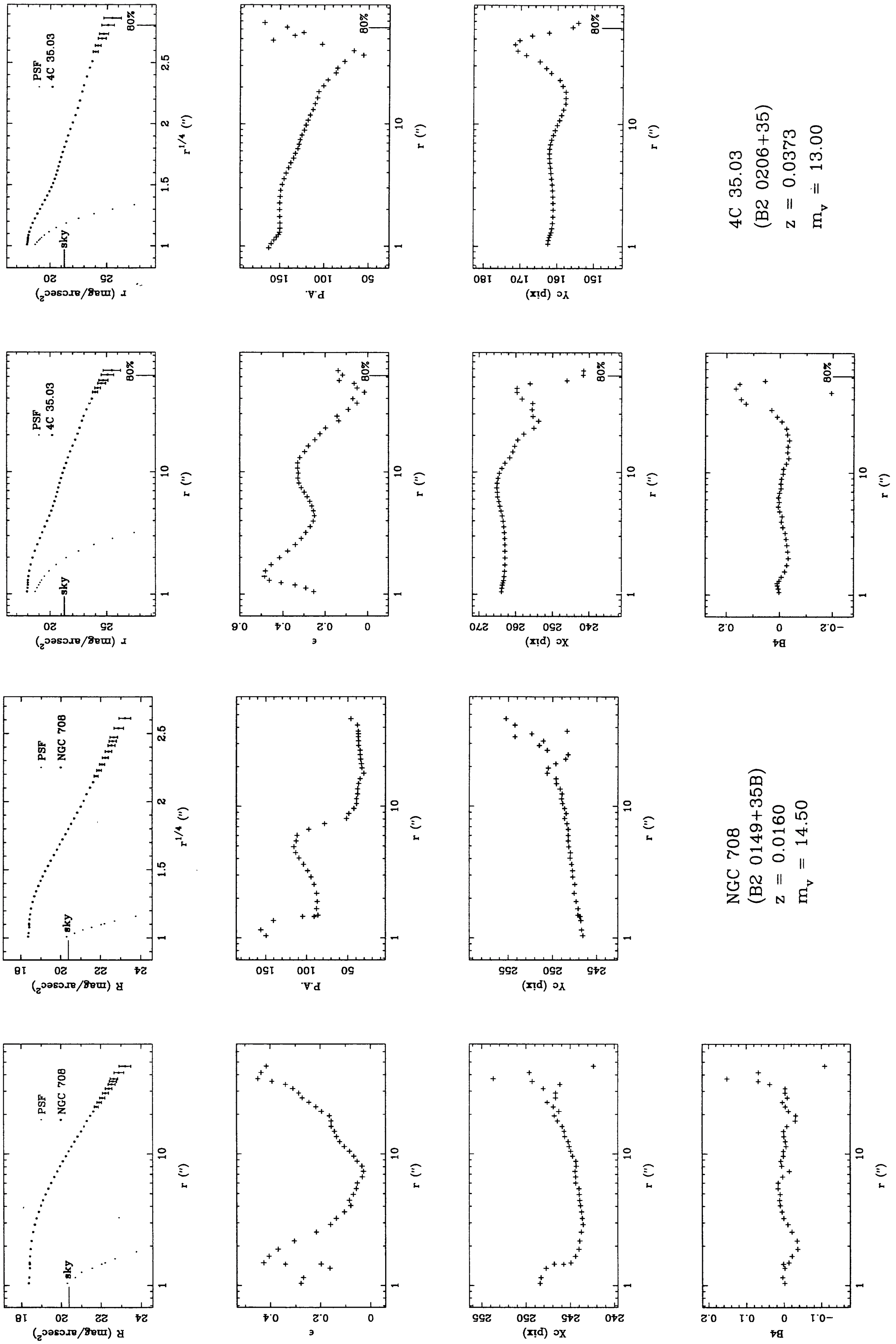

FIG. 2—*Continued*

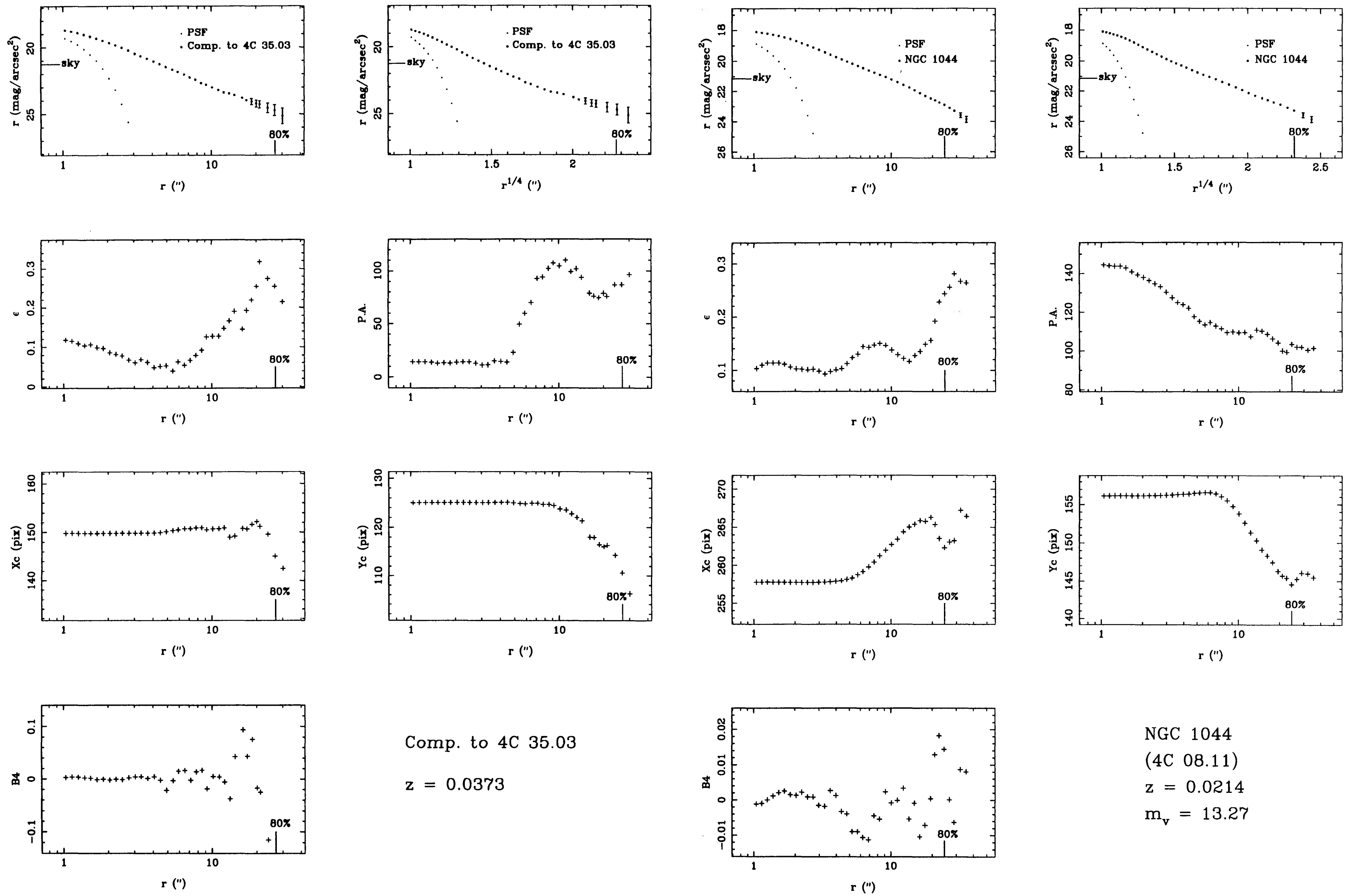

FIG. 2—*Continued*

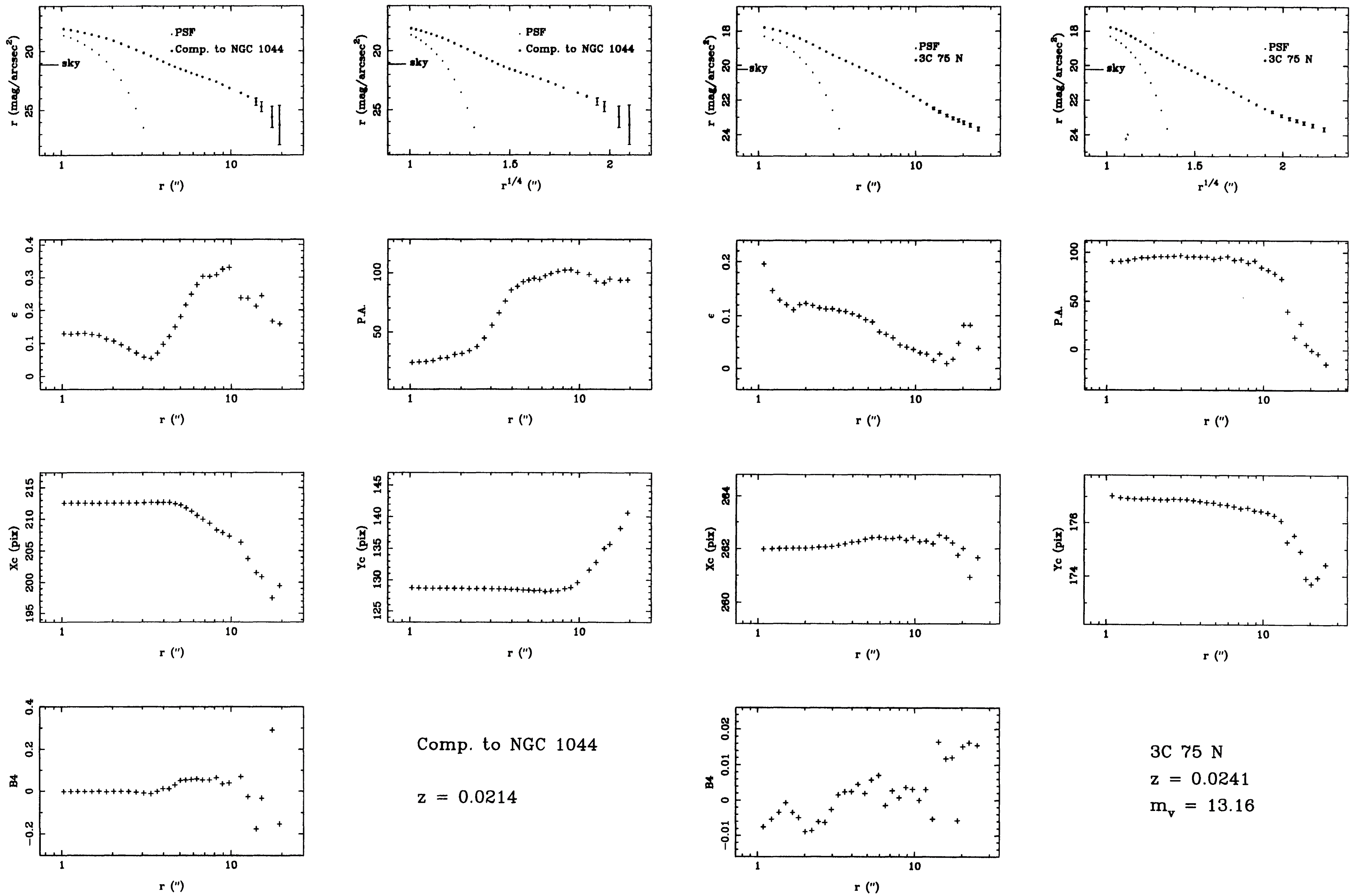

FIG. 2—*Continued*

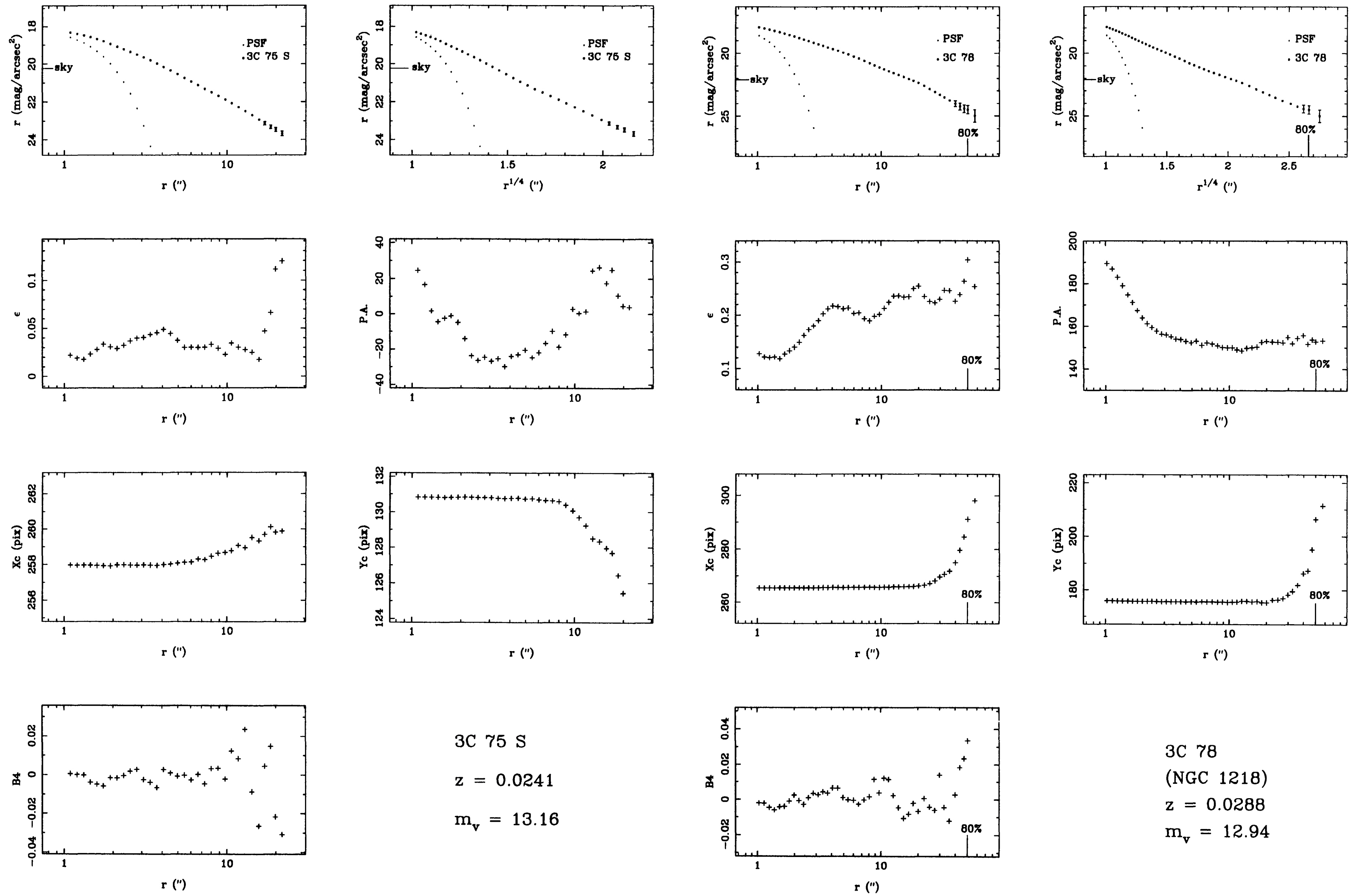

FIG. 2—*Continued*

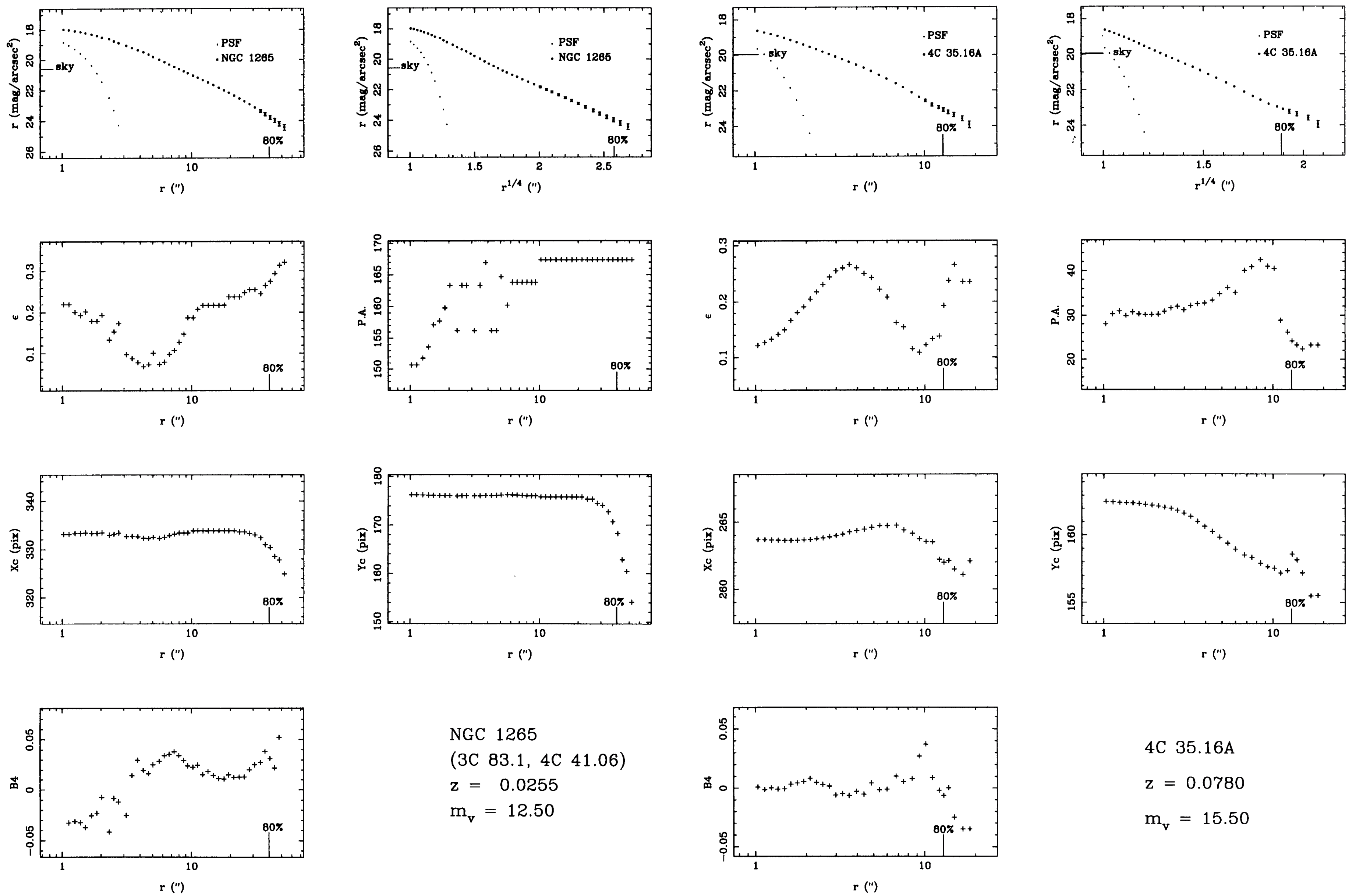

FIG. 2—*Continued*

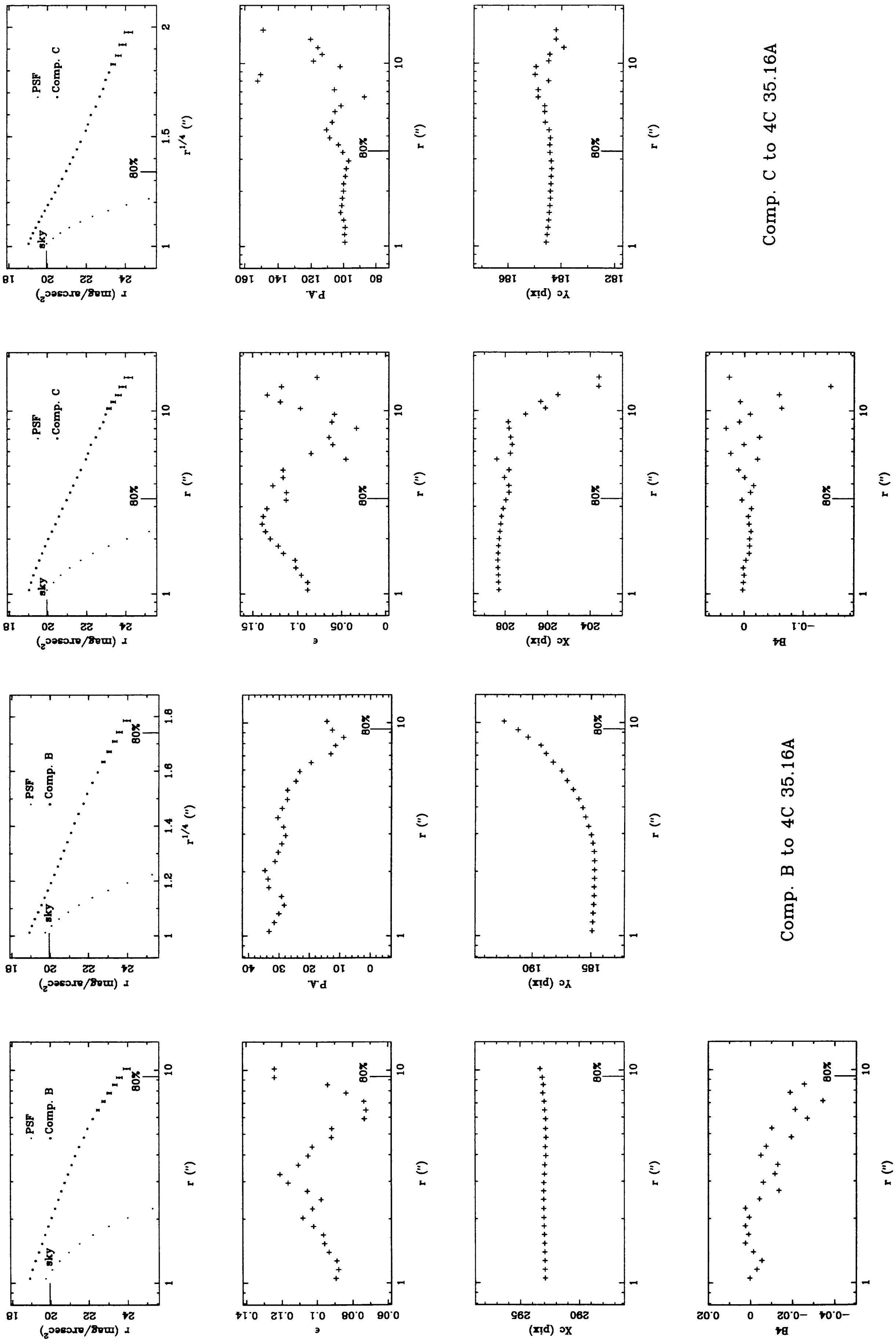

FIG. 2—*Continued*

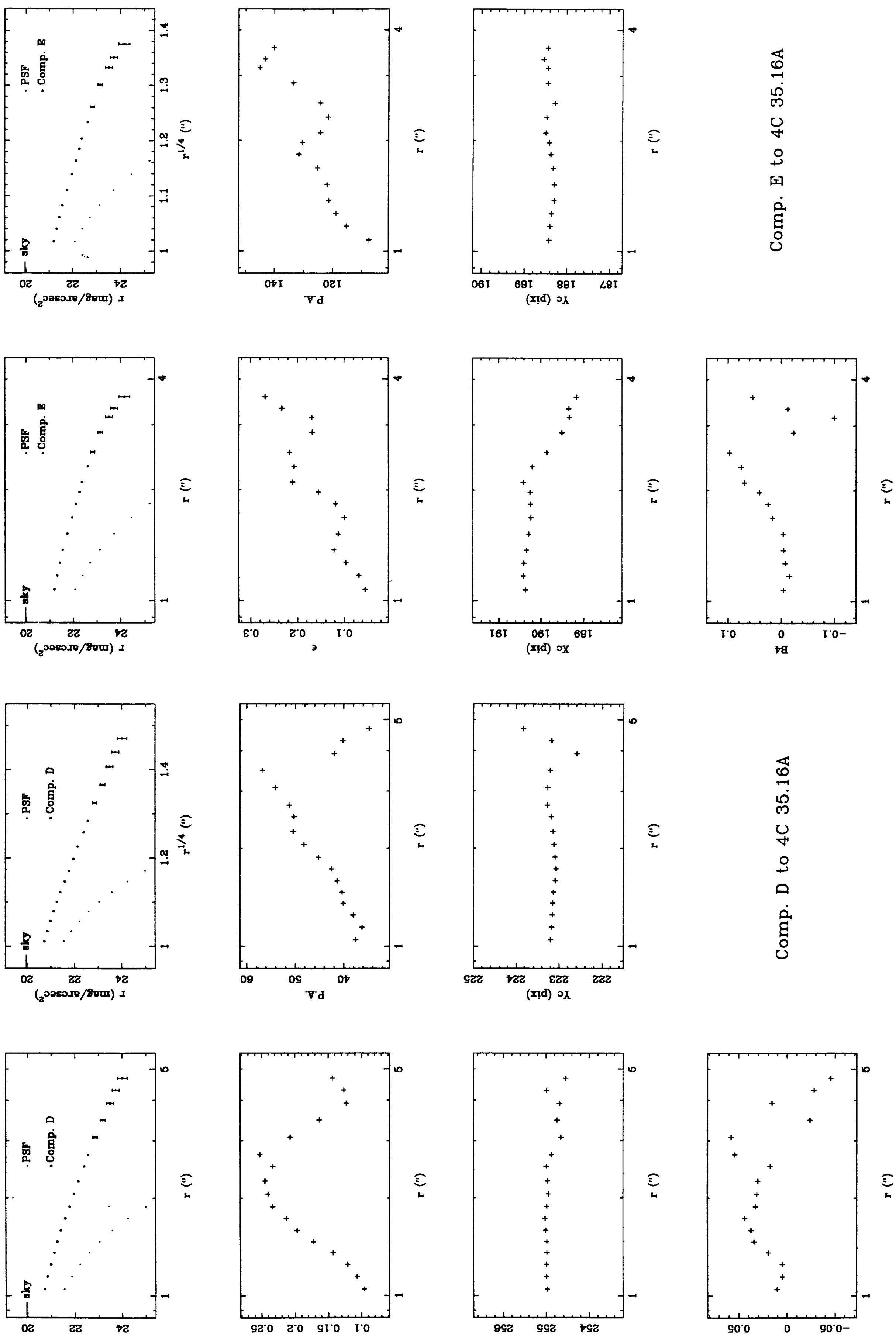

FIG. 2—*Continued*

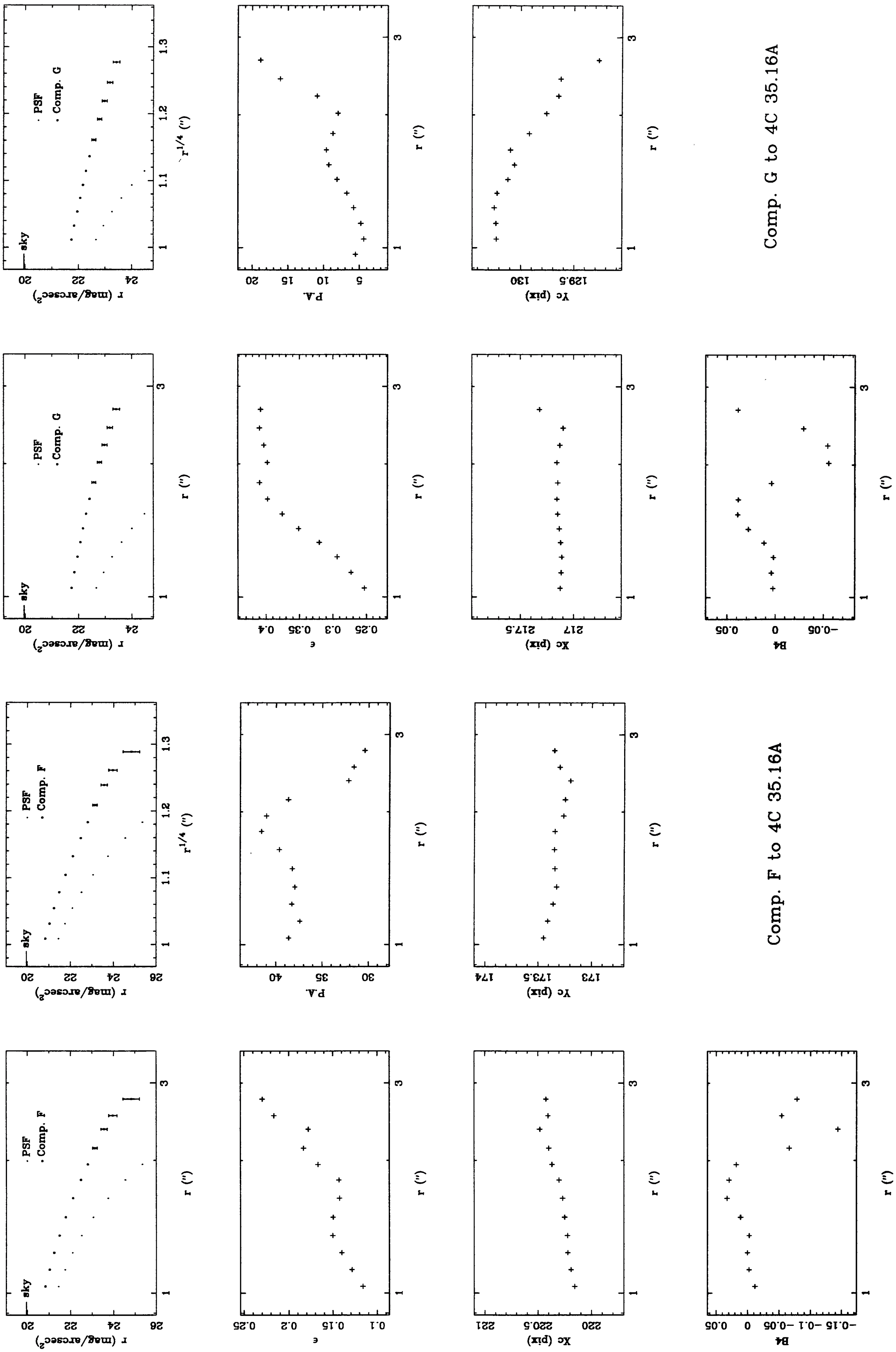

FIG. 2—*Continued*

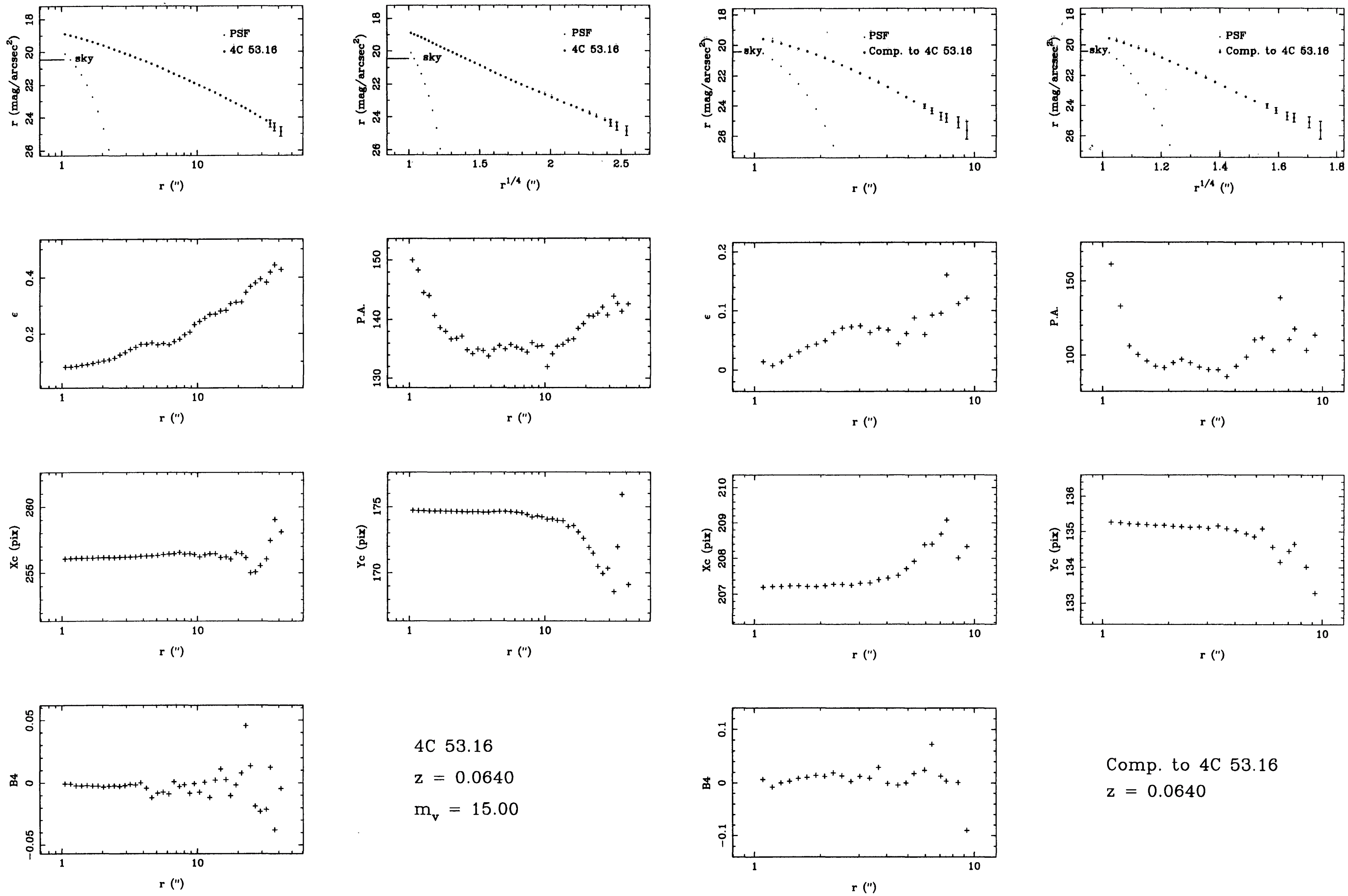

FIG. 2—*Continued*

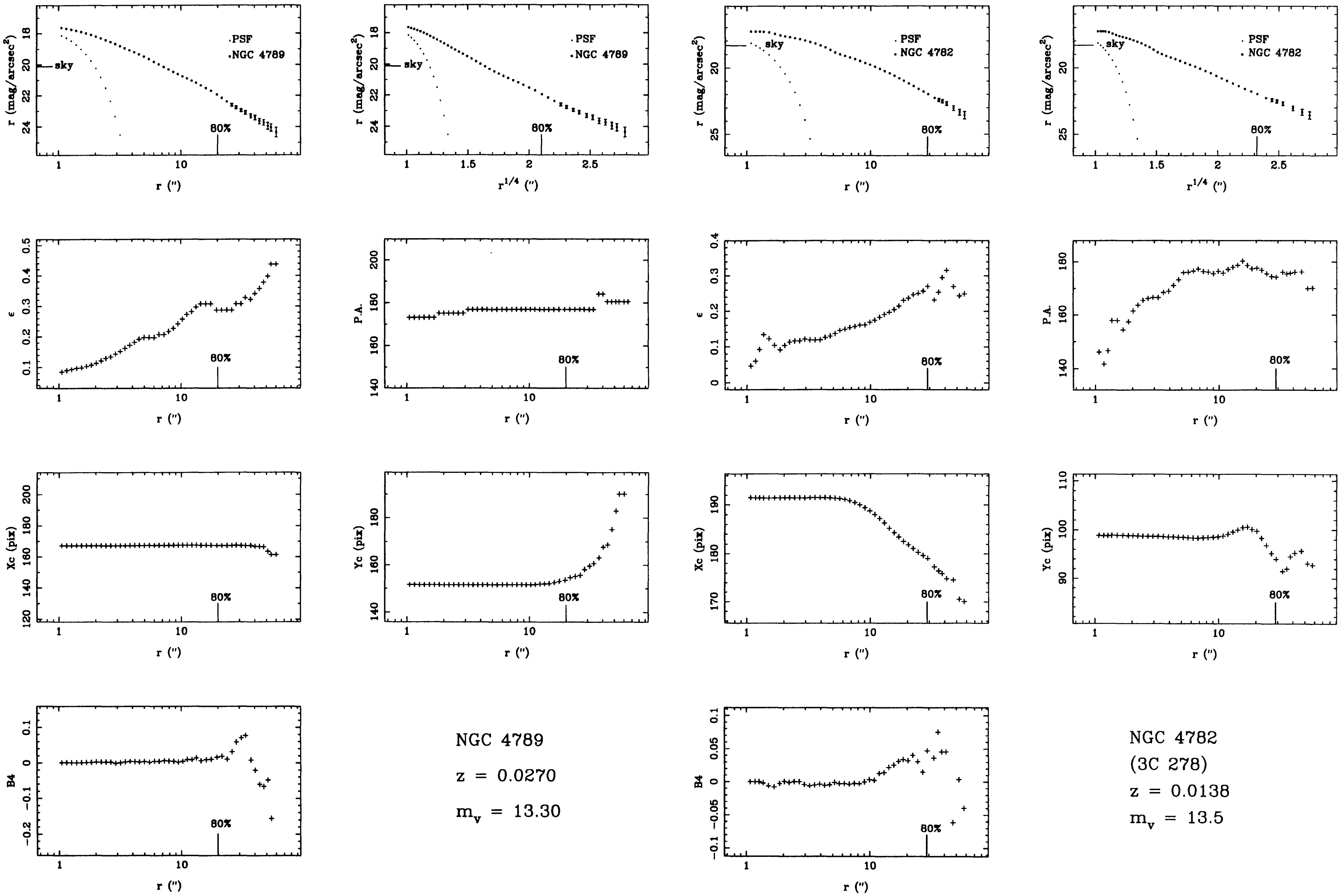

FIG. 2—*Continued*

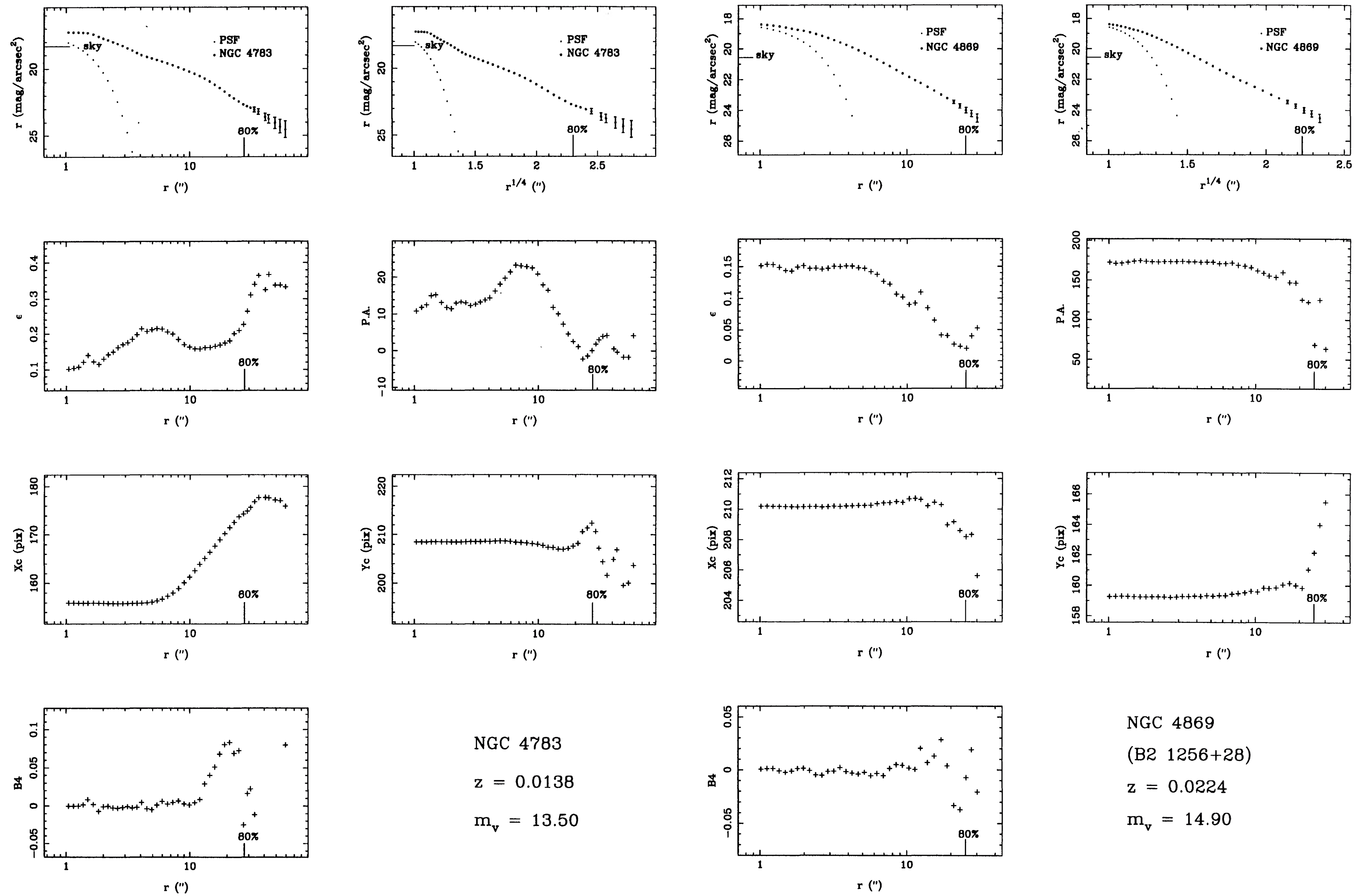

FIG. 2—*Continued*

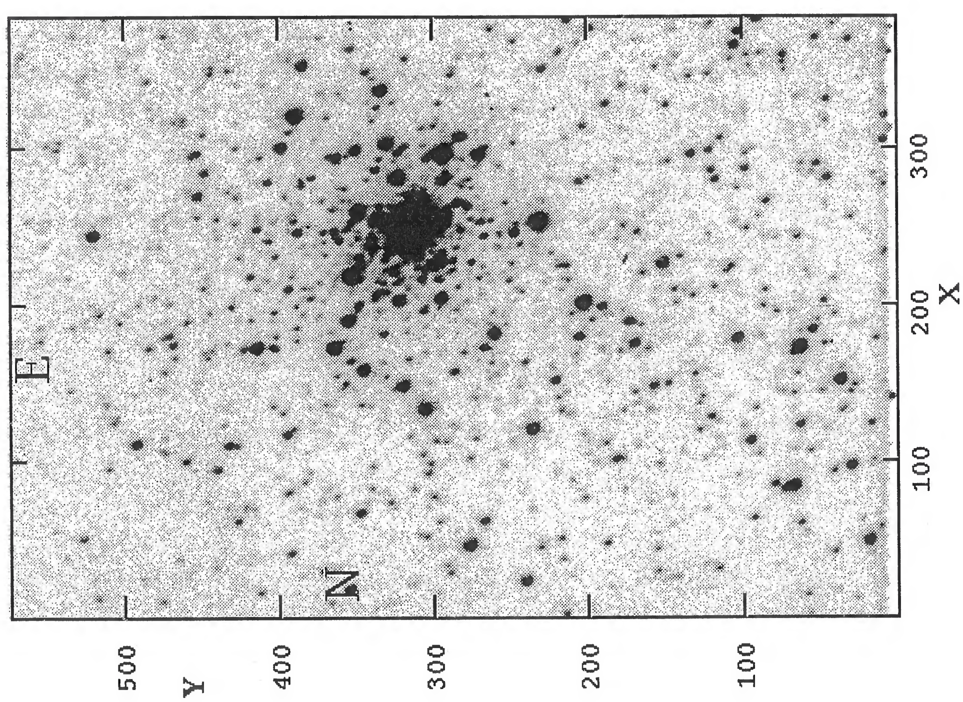
Y
X
N
E
500
400
300
200
100
100
200
300

FIG. 1g

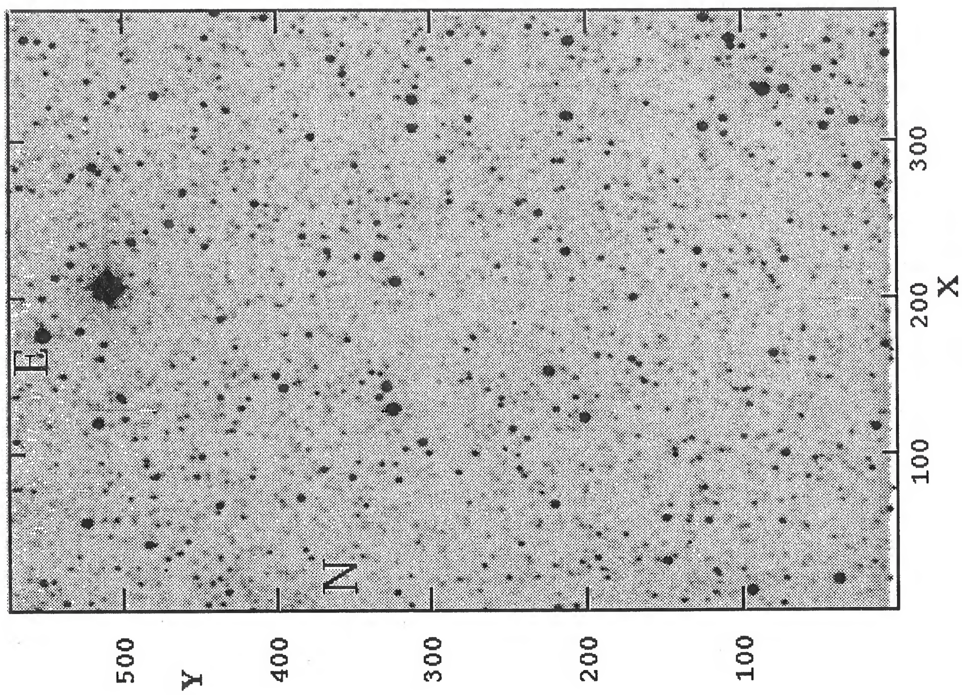
Y
X
N
E
500
400
300
200
100
100
200
300

FIG. 1h

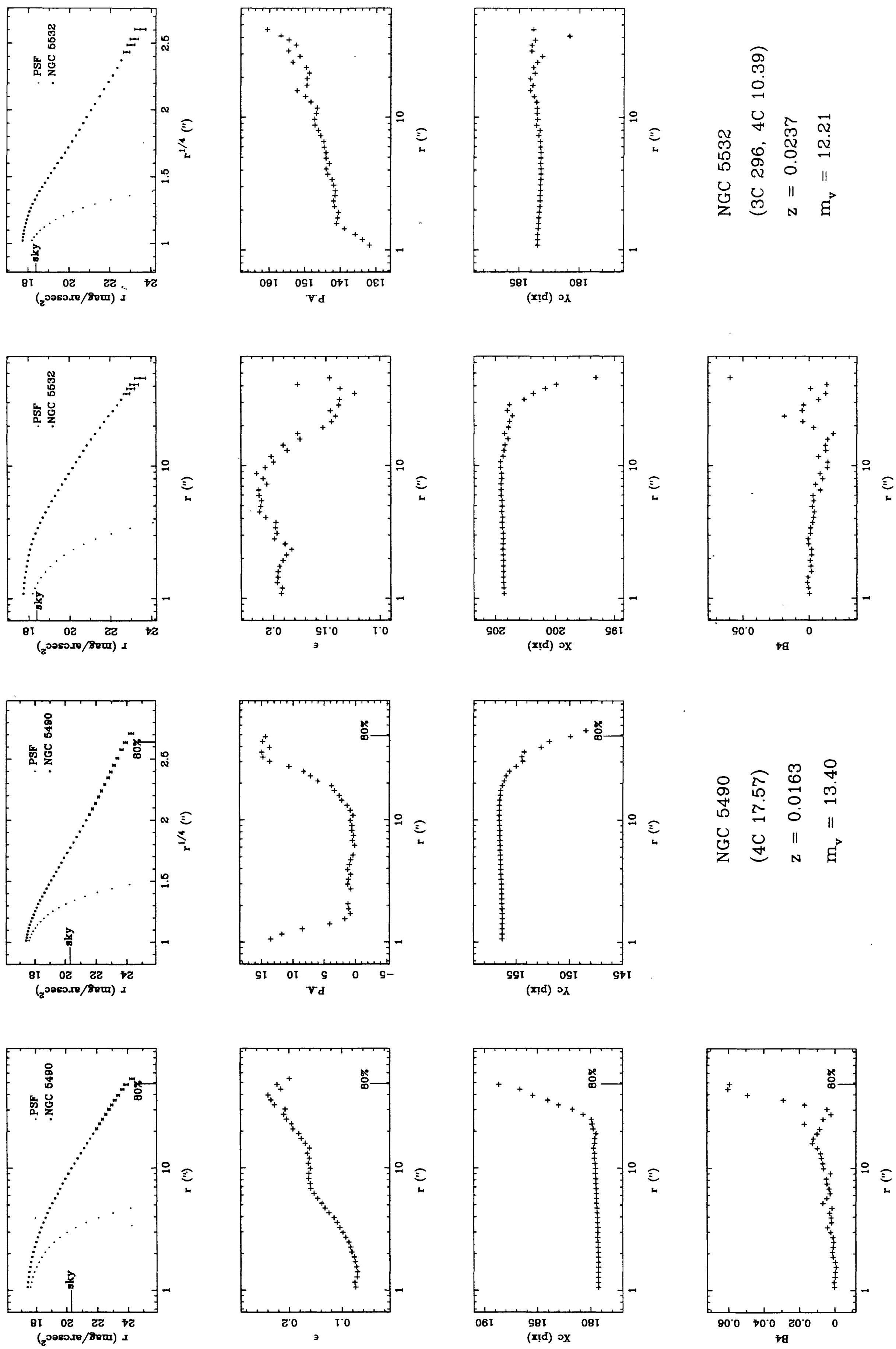

FIG. 2—*Continued*

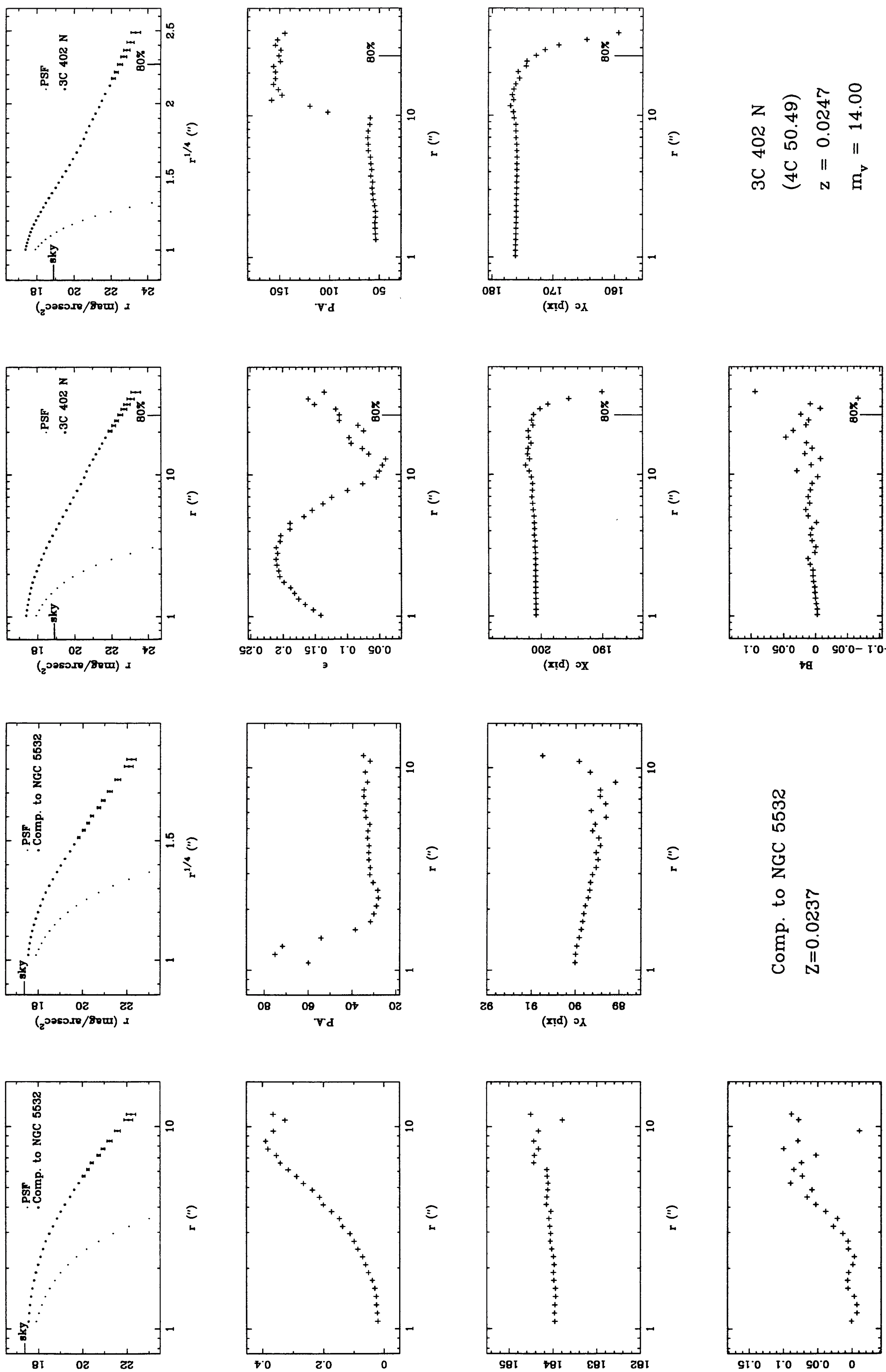

FIG. 2—*Continued*

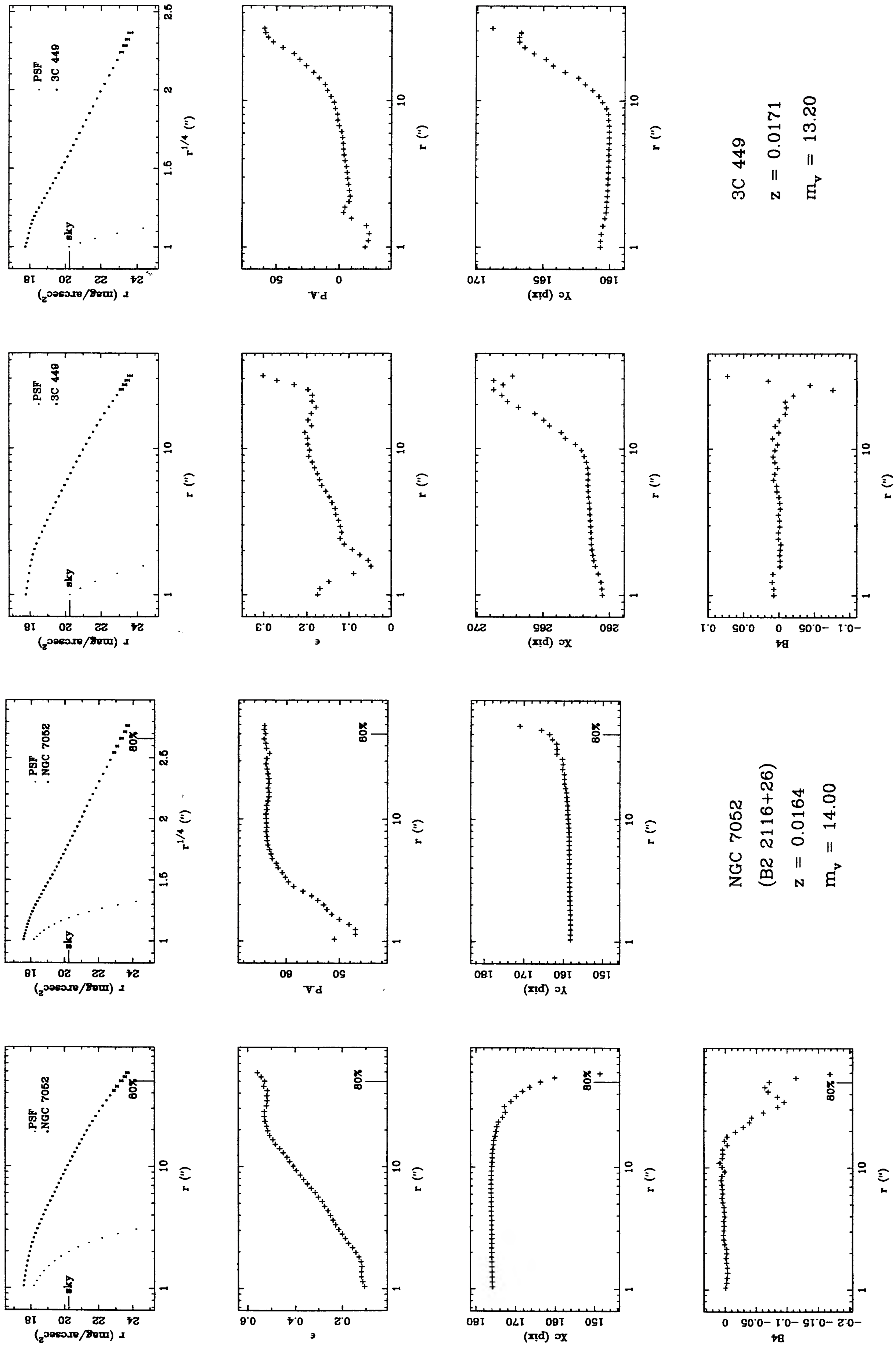

FIG. 2—*Continued*

1994ApJS...91..507D

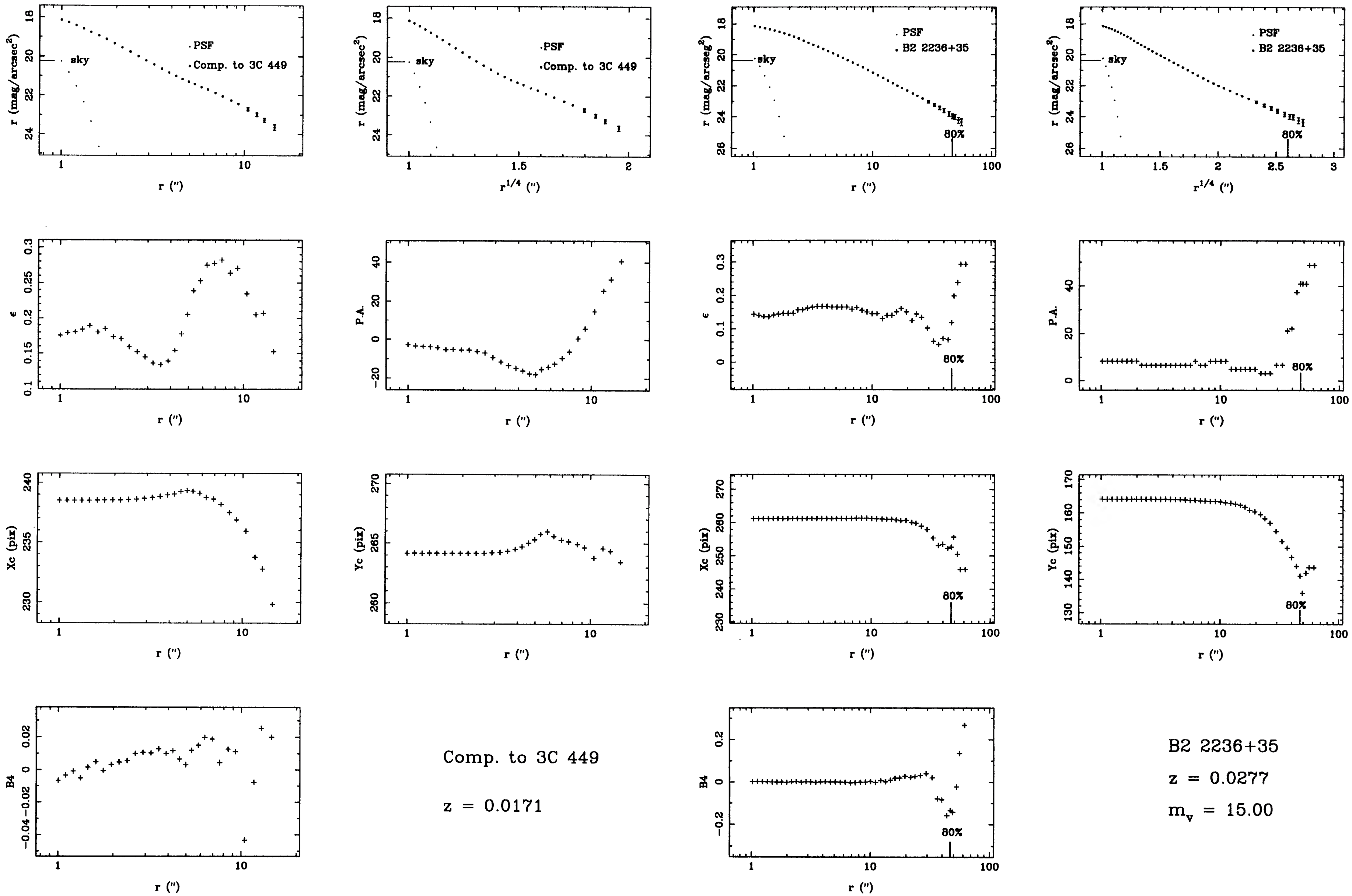

FIG. 2—*Continued*

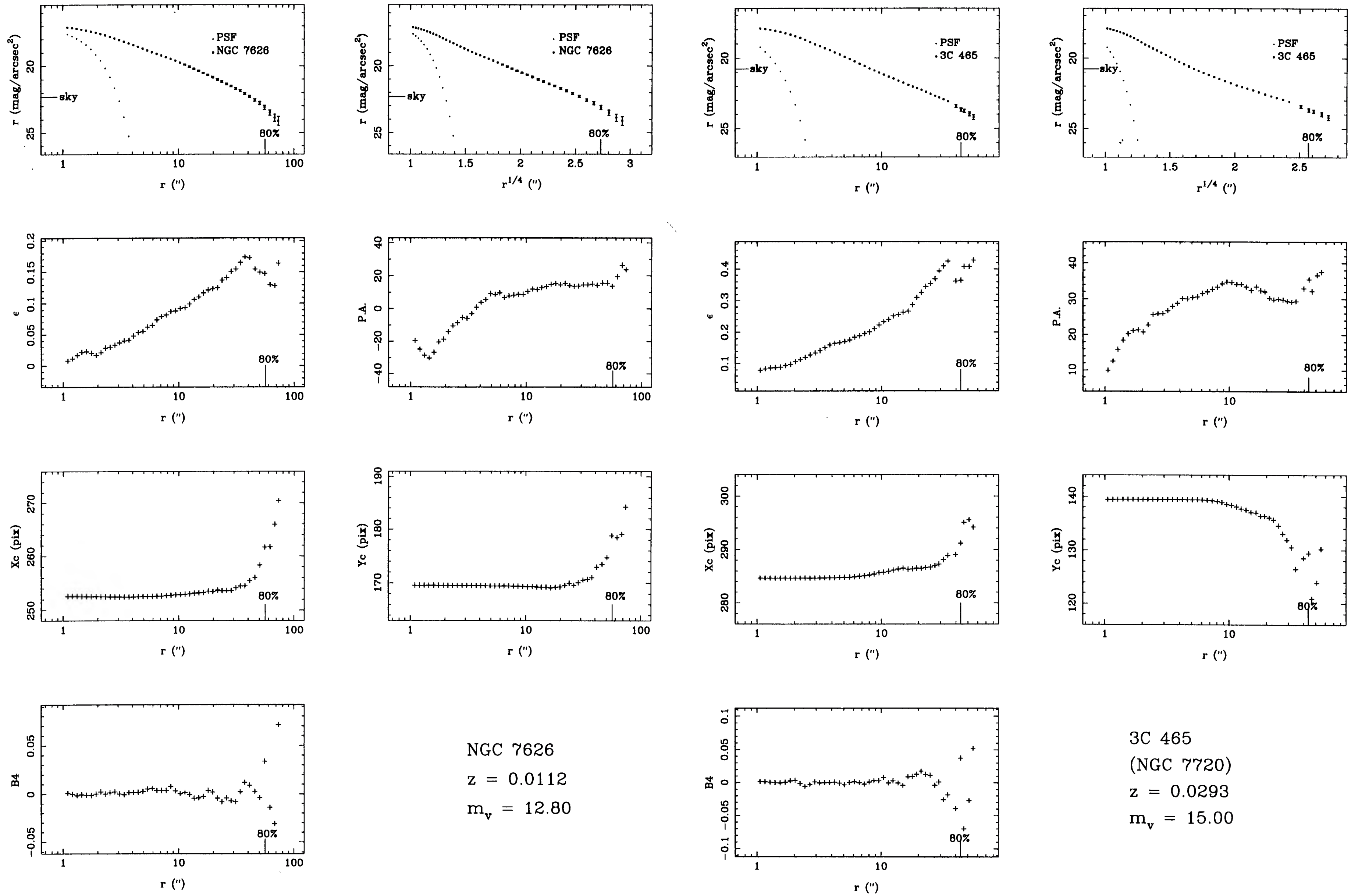

FIG. 2—*Continued*

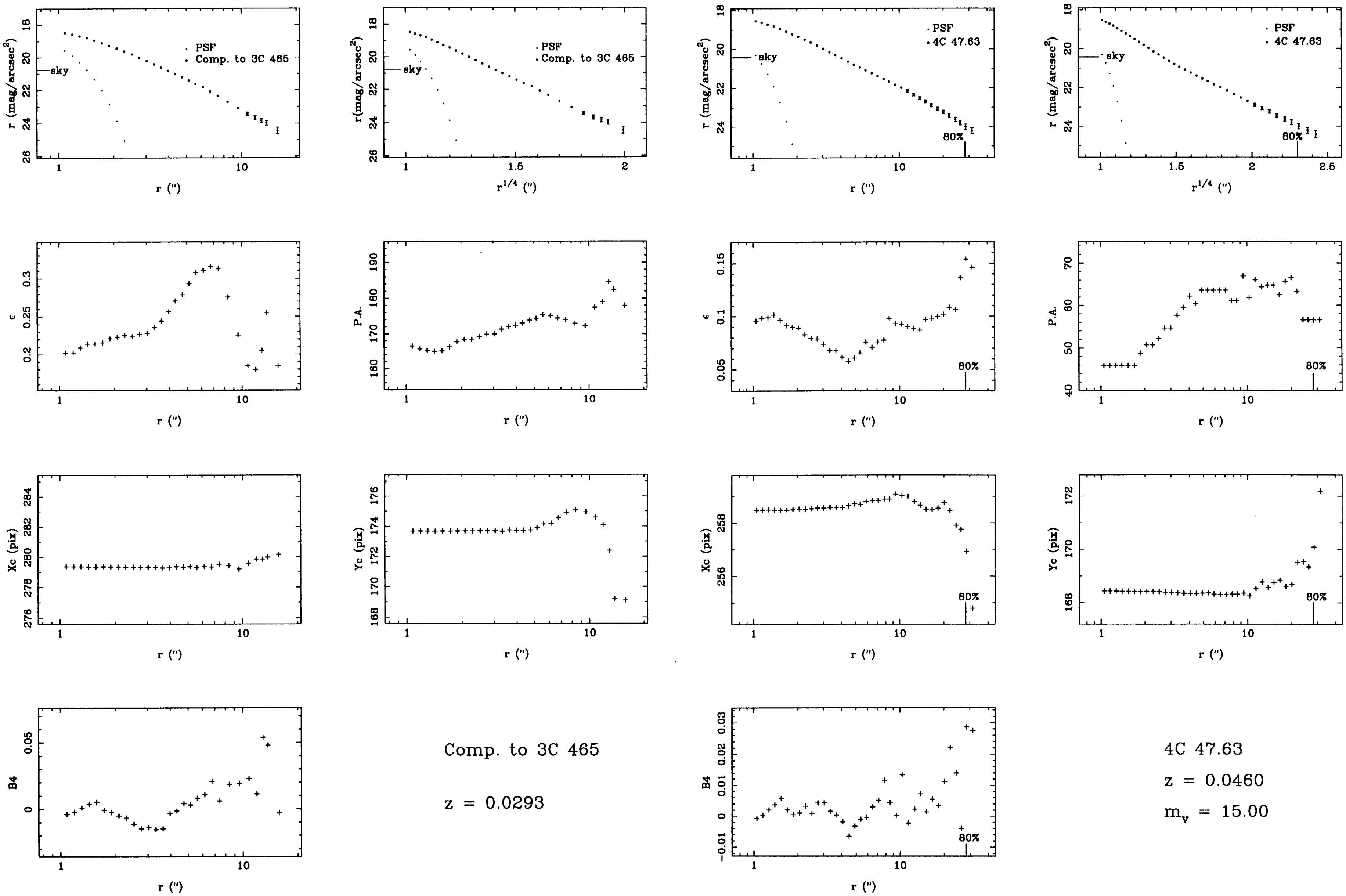

FIG. 2—*Continued*

TABLE 2

SAMPLE[a]

ISOPHOTE FITTING PARAMETERS

r (″)	r (mag/arcsec^2)	ϵ	P.A. (degrees)	X_0 (pix)	Y_0 (pix)	B_4 (x10^{-3})
1.00	17.66 ± 0.04	0.172	−41.3	255.2	169.4	0.8
1.09	17.66 ± 0.04	0.196	−26.4	255.2	169.4	−3.2
1.21	17.67 ± 0.04	0.181	−12.2	255.2	169.3	−0.3
1.36	17.68 ± 0.04	0.136	26.3	254.9	169.5	−1.0
1.47	17.68 ± 0.04	0.171	32.9	254.8	169.5	−0.9
1.55	17.69 ± 0.04	0.232	40.5	254.7	169.6	0.8
1.67	17.69 ± 0.04	0.272	43.1	254.7	169.4	1.9
1.87	17.70 ± 0.04	0.239	44.2	254.6	168.9	−2.7
2.11	17.75 ± 0.04	0.205	41.0	254.5	168.7	−1.2
2.32	17.82 ± 0.04	0.204	38.2	254.5	168.6	1.0
2.54	17.90 ± 0.04	0.209	39.1	254.5	168.6	−2.8
2.77	17.98 ± 0.04	0.224	40.0	254.5	168.6	−2.6
3.03	18.08 ± 0.04	0.232	40.1	254.5	168.6	−0.8
3.31	18.18 ± 0.04	0.240	41.0	254.5	168.7	−2.5
3.64	18.28 ± 0.04	0.245	42.1	254.5	168.7	−6.8
3.99	18.38 ± 0.04	0.248	42.9	254.5	168.7	−11.7
4.37	18.49 ± 0.04	0.255	44.2	254.5	168.8	−13.7
4.79	18.59 ± 0.04	0.260	44.3	254.5	168.8	−12.3
5.23	18.70 ± 0.04	0.271	45.0	254.6	168.8	−11.0
5.74	18.87 ± 0.04	0.273	45.2	254.7	168.8	−3.9
6.30	19.00 ± 0.04	0.278	45.7	254.8	168.8	−6.9
6.90	19.13 ± 0.04	0.284	45.3	254.8	168.8	−4.0
7.59	19.26 ± 0.04	0.283	45.2	254.8	168.8	−7.3
8.34	19.40 ± 0.04	0.285	44.5	254.9	168.7	−9.0
9.14	19.53 ± 0.04	0.291	44.3	254.9	168.6	−8.7
10.01	19.66 ± 0.04	0.297	44.9	254.9	168.6	−10.9
11.01	19.80 ± 0.04	0.296	44.7	255.0	168.5	−11.9
12.11	19.94 ± 0.04	0.296	44.2	255.0	168.4	−13.3
13.34	20.09 ± 0.04	0.295	44.0	254.8	168.5	−12.4
14.78	20.25 ± 0.05	0.285	43.9	254.9	168.5	−10.1
16.36	20.42 ± 0.05	0.275	44.3	254.9	168.3	−5.7
18.03	20.59 ± 0.05	0.273	44.0	254.9	168.3	−5.6
19.98	20.77 ± 0.05	0.262	44.2	254.9	168.3	−7.2
22.05	20.96 ± 0.05	0.257	44.2	254.8	168.1	−4.1
24.29	21.14 ± 0.05	0.255	43.9	254.9	168.1	−5.6
26.75	21.33 ± 0.05	0.253	44.3	254.9	168.0	−1.0
29.30	21.50 ± 0.05	0.259	44.1	254.8	167.8	−3.8
32.16	21.68 ± 0.05	0.263	44.6	254.7	167.7	−3.3
35.50	21.88 ± 0.05	0.258	45.4	254.2	168.0	−2.4
38.80	22.07 ± 0.06	0.267	43.3	253.4	166.8	−3.4
42.82	22.27 ± 0.06	0.262	44.0	253.8	167.0	−9.1
47.43	22.50 ± 0.06	0.252	44.0	252.7	166.2	−9.6
52.44	22.75 ± 0.07	0.244	44.6	252.3	165.0	3.0
58.42	23.11 ± 0.08	0.225	50.4	251.6	166.0	105.4
64.55	23.45 ± 0.10	0.218	52.1	249.1	161.4	128.4
72.80	23.87 ± 0.13	0.178	56.5	244.8	157.6	246.2
82.95	24.35 ± 0.19	0.118	42.6	245.1	147.7	829.9

[a] This sample shows parameters for NGC 315. Table 2 is published in its entirety in computer-readable form on the AAS CD-ROM Series, Vol. 2.

there are some perturbation in the parameters of 4C 35.03 (specially in the inner regions) caused by this secondary nucleus. Similar problems were found in González-Serrano & Pérez-Fournon (1991). These authors presented profiles of V surface brightness, ellipticity, position angle, B_3 and B_4 Fourier coefficients, and a parameterization of isophote displacements for both galaxies. All these profiles are comparable to ours.

The position angle of the main galaxy shows strong twisting from the inner (P.A. ~ 150°) to the outer parts (P.A. ~ 60° at $r = 40''$). The isophote centers are displaced toward the NE in the inner 40″ ($\Delta r \sim 3''.7$).

The companion shows also strong isophote twists (ΔP.A. ~ 90° at $r = 10''$) and off-centering: the centers move to the south, with $\Delta r \sim 3''.2$ at $r = 20''$.

NGC 1044.—This system consists of the galaxy NGC 1044, which is the optical counterpart of the radio source (Burns et al. 1987), and its companion at P.A. 122° (at a projected distance of 4″.4). They are located in the Zwicky cluster 0238.4+0831. These two galaxies are almost aligned with a third one at P.A. 305°.

The parameters of both galaxies show the following features:

1. NGC 1044 B shows gradients in ellipticity larger than in normal ellipticals. Ellipticity has a minimum at $r \sim 3''.4$, increasing then up to 0.33 at $r \sim 10''$ ($\Delta\epsilon \sim 0.28$).

2. Both galaxies show isophote twists: ΔP.A. ~ 30° in NGC 1044 A (between $r \sim 3''$ and 20″) and ~34° in the companion (between $r \sim 3''$ and 10″).

3. Nonconcentric isophotes: The isophote centers of the main galaxy are strongly displaced to the SW (e.g., isophotes at $r \sim 20''$ are displaced 4″.6 from the nucleus). Those of the secondary are displaced to the NE (about 1″.9 from the nucleus at $r \sim 10''$.

3C 75.—The host galaxy is a dumbbell system located in the central region of the Abell cluster A400. Lauer (1988) gives r-brightness profiles for both galaxies, assuming concentric isophotes, while Smith & Heckman (1989b) give azimuthally averaged V-profiles.

The radio source shows a complex jet structure (Owen et al. 1985).

The following are the main features of these galaxies:

1. Twist of their isophotes. The position angle of 3C 75N appears to decrease from ~90° in the inner 9″ to ~−10° outward, pointing approximately to the companion. In 3C 75S the P.A. varies from ~−20° in the inner 5″ to ~20° at 15″.

2. Nonconcentric isophotes. The outer isophotes of 3C 75 S at ~18″ are displaced by ~1″.7 from the nucleus in the direction SW. The outer envelope of 3C 75 N at the same distance is shifted by ~1″ from the nucleus toward SW.

4C 35.16.—This small group of galaxies located in the Abell cluster A568, shows a rather complex structure, both at optical and at radio frequencies (see radio map in Giovannini, Feretti, & Gregorini 1987).

The main optical system consists of galaxies A and B, being the latter at P.A. 309° with respect to the nucleus of A. The system consists of other five smaller galaxies (C–G) located at positions 68°, 10°, 71°, 76° and 124°, respectively.

Galaxies A and B show the most interesting optical features: Both of them show twist of their isophotes, ΔP.A. ~ 20°. The outer isophotes of galaxy A, at 12″, are off-centered, with respect to the inner ones, by $\Delta r \sim 1''.8$. Galaxy B also shows displacements of its isophote centers: at 9″, the center has moved by ~1″.7 toward the north.

The results for galaxies D–G must be carefully considered: their sizes are comparable to seeing disk size (FWHM ~ 1″.6).

4C 53.16.—The host galaxy is the dominant member of the Zwicky cluster 0712.9+5334. It has a small companion at P.A. 127°. The radio source (Burns & Gregory 1982) is associated with the main galaxy.

The main galaxy has quite large displacements of its isophotes toward the south, with $\Delta r \sim 0''.9$ at $r \sim 20''$. The companion has also shifts of its isophote centers: $\Delta r \sim 0''.6$ at $r \sim 7''$.

3C 278.—This wide-angle tail radio source (Baum et al. 1988) is associated with the southern component (NGC 4782) of the dumbbell system NGC 4782/4783. At optical wavelengths, it has been analyzed by several authors: Smith & Heckman (1989b) give an azimuthally averaged V brightness profile of NGC 4782; Madejsky, Bender, & Möllenhoff (1991) give the same kind of profile as Smith and Heckman but using a similar decomposition algorithm as in this work, and also, isophote displacements for both galaxies; both results are in agreement with ours.

In NGC 4782 the position angle changes by $\sim 10°$ from $r = 3''$ to $30''$. In the companion, ΔP.A. $\sim 20°$ from $r = 5''$ to $30''$. Both galaxies also show strong shifts of their isophotes: e.g., at $r \sim 30''$ the isophote centers of NGC 4782 are displaced by 4″.6 to the east; in NGC 4783, this shift corresponds to 6″.7 to the west.

NGC 4869.—This galaxy is located in the central region of the cluster Coma (A1656). It has a small companion located in position P.A. 325°. The radio map given in O'Dea & Owen (1985) shows the twin-tail structure of the radio source.

The position angle of the main galaxy has a large decrease, with ΔP.A. $\sim 50°$ at $r = 23''$. The isophote centers are displaced to the NE, with $\Delta r \sim 0''.87$ at $r = 23''$.

In the companion there are also P.A. twists and isophotes displacements. The position angle has changed about 40° at $r = 8''$, and $\Delta r \sim 1''.0$ at the same radius.

3C 402 N.—It presents a two-sided jet structure, at a P.A. of about 175° (Riley & Pooley 1975). The CCD image shows a star near the nucleus of the galaxy, and two smaller companions located along P.A. 151° and P.A. 341°.

The parameters of this galaxy show these features:

1. Ellipticity profile appears quite different from the rest of the sample and from those typical in ellipticals. Ellipticity decreases by $\Delta\epsilon \sim 0.17$ reaching a minimum at $r \sim 13''$ and increasing from this point onward.

2. The position angle profile shows an abnormal behavior, increasing sharply by $\sim 90°$ between $r \sim 10''$–$13''$.

3. Isophote centers are slightly displaced by $\sim 1''.4$ to the NW, just in the region at $r \sim 10''$–$13''$.

NGC 7052.—This is an isolated galaxy with a dust lane oriented along the optical major axis (Nieto et al. 1990). At optical wavelengths, the following information can be found in the literature: Lauer (1985) gave ellipticity and position angle for the core and R brightness profile assuming concentric isophotes; Bender et al. (1988) presented profiles of ellipticity, position angle, and B_3 and B_4 Fourier coefficients (called A_3 and A_4 in their work); González-Serrano (1989) presented profiles of V surface brightness, ellipticity, position angle, and B_4 Fourier coefficient. All these results agree with ours.

The radio morphology consists of a symmetric double jet in positions P.A. 21° and P.A. 201° (Morganti et al. 1987).

It shows strong outer boxy isophotes as many other authors have reported (e.g., Lauer 1985; Bender et al. 1988), from $r \sim 18''$ outward. This causes a high negative value of fourth cosine coefficient, B_4 and a large variation in ellipticity in the model fit (from 0.2 at $r \sim 30''$ to 0.5 at $r \sim 3''$).

3C 449.—The system consists of the main galaxy and a nearby companion located at 37″.4 in P.A. 13°. They both are members of the Zwicky cluster 2231.2+3732. The radio source, which is associated with the main galaxy, shows two symmetric jets along directions P.A. 13° and P.A. 186° (Perley et al. 1979). At optical wavelengths, the main component has been previously analyzed by Smith & Heckman (1989b), who gave profiles of V-magnitude, ellipticity, and position angle. Their results are in agreement with ours.

The parameters of the main galaxy show discontinuities around $r \sim 2''$, most likely due to the presence of a ring of absorbing material at $r \sim 2''$ (Butcher et al. 1980). The main features are listed below:

1. Large gradients in ellipticity. In the host galaxy, ellipticity gradients are slightly higher than in normal ellipticals, with $\Delta\epsilon \sim 0.25$. In the companion, ellipticity shows an abnormal behavior, decreasing in the region inner to $r \sim 3''.5$, then increasing by $\Delta\epsilon \sim 0.16$ from $r \sim 3''.5$–$7''.5$ and beginning to decrease beyond that radius.

2. Strong isophote twist. In the main galaxy, P.A. varies from $-10°$ to $5°$ within the first $10''$. Then, P.A. increases strongly up to 50° at $r \sim 25''$. The P.A. of the companion shows a decrease of $\sim 20°$ in the inner $5''$, and then increases $\sim 40°$.

3. Nonconcentric isophotes. The isophotes of the main galaxy at $r \sim 10''$–$25''$ are displaced to the NW $\sim 3''.2$ from the nucleus. The off-centering coincides in amplitude and distance to the center with the strongest change in P.A. In the companion, the isophote center shows a displacement by $\sim 0''.7$ toward the east at a distance of $r \sim 10''$ from its nucleus.

B2 2236+35.—Located in the Zwicky cluster 2231.2+3732, this galaxy has a symmetric double jet along P.A. 46° (Morganti et al. 1987). Our CCD image shows a companion at P.A. 55°. The wide optical bands which appear in the outer isophotes in positions P.A. 85° and P.A. 255° are due to spurious reflections. González-Serrano (1989) gives ellipticity, position angle, B_4, and V brightness profiles that are in good agreement with ours.

The resulting parameters for the outer contours (namely $r > 33''$) must be carefully taken into account because of the presence of the reflections. However, the isophote displacements seem to be real: those at $r \sim 33''$ are displaced $\sim 5''$ from the nucleus to the SE.

3C 465.—This radio source is associated with the optical galaxy NGC 7720, which is the brightest member of the cluster Abell 2634. It has a companion along P.A. 10°. Lauer (1988) gives r brightness profiles for both components (assuming concentric isophotes). The radio emission presents a wide-angle tail morphology (Eilek et al. 1984).

The structural parameters of the main galaxy are listed below:

1. High gradients in ellipticity: it varies from 0.1 to 0.4 between $r \sim 2''$–$30''$.

2. Nonconcentric isophotes. They appear to have a common center until $r \sim 8''$. Then, the isophote center moves by $\sim 5''$ toward the SW.

NGC 7626.—It is one of the two brightest ellipticals in the Pegasus I cluster. The radio source associated to it consists of two strong well defined radio jets along P.A. 35° (Birkinshaw & Davies 1985).

Some optical properties of the host galaxy can be found in the literature: Lauer (1985) presented ellipticity, position angle, and R brightness profiles, evaluated assuming concentric isophotes; Bender et al. (1988) gave profiles of ellipticity, position angle, and B_3 and B_4 Fourier coefficients; Franx et al. (1989) and Peletier et al. (1990) presented profiles of ellipticity, position angle, R-magnitude, $U - R$ and $B - R$ colors, and Fourier coefficients of third and fourth order; Sparks et al. (1991) gave B, V, I surface brightness profiles as well as ellipticity, position angle, B_4, and isophote displacements. All of the results from these authors are in good agreement with ours.

We have not observed the excess light reported by Forbes & Thomson (1992). These authors, using a masking-method different from ours, found a region at the SW with an excess light which could be due to tidal effects (possibly with the brighter giant elliptical NGC 7619 located at the west).

4C 47.63.—This radio galaxy has two well defined jets emerging from its nucleus in directions P.A. 58° and P.A. 218° (Burns & Gregory 1982). It is located in the Zwicky cluster 2354.1+4719.

The parameters show these features:

1. Twist of the isophotes: P.A. changes ~20° from 2″ to 5″.
2. There is also a change of the sign in fourth cosine factor, B_4, in the same region where ellipticity has its minimum and P.A. tends to increase.

5. CONCLUSIONS

We have obtained the radial dependence of parameters like the surface brightness, ellipticity, center and position angle of 25 low-luminosity elliptical radio galaxies, using a numerical method based on elliptical fitting to their isophotes. We have also been able to analyze pairs or groups of galaxies of the sample applying an iterative decomposition method. We have detected that 60% of the galaxies in the present sample show distortions in their structural parameters (isophote twists, non-concentric isophotes) not found in isolated ellipticals. These distortions are especially important in the case of galaxies with a close companion or in dumbbell systems (NGC 326, 3C 31, 4C 35.03, NGC 1044, 3C 75, 4C 35.16, NGC 4782/3, 3C 449, and 3C 465).

It is a pleasure to thank Ignacio González-Serrano for permission to use his improved version of the GASP package. This work has been partially supported by the grant DGYCIT PB900182.

APPENDIX
TESTING THE ITERATIVE DECOMPOSITION METHOD

Pairs or groups of galaxies have been analyzed in an iterative way, as explained above (§ 3.3). We have checked the validity of this procedure applying it to several simulated pairs.

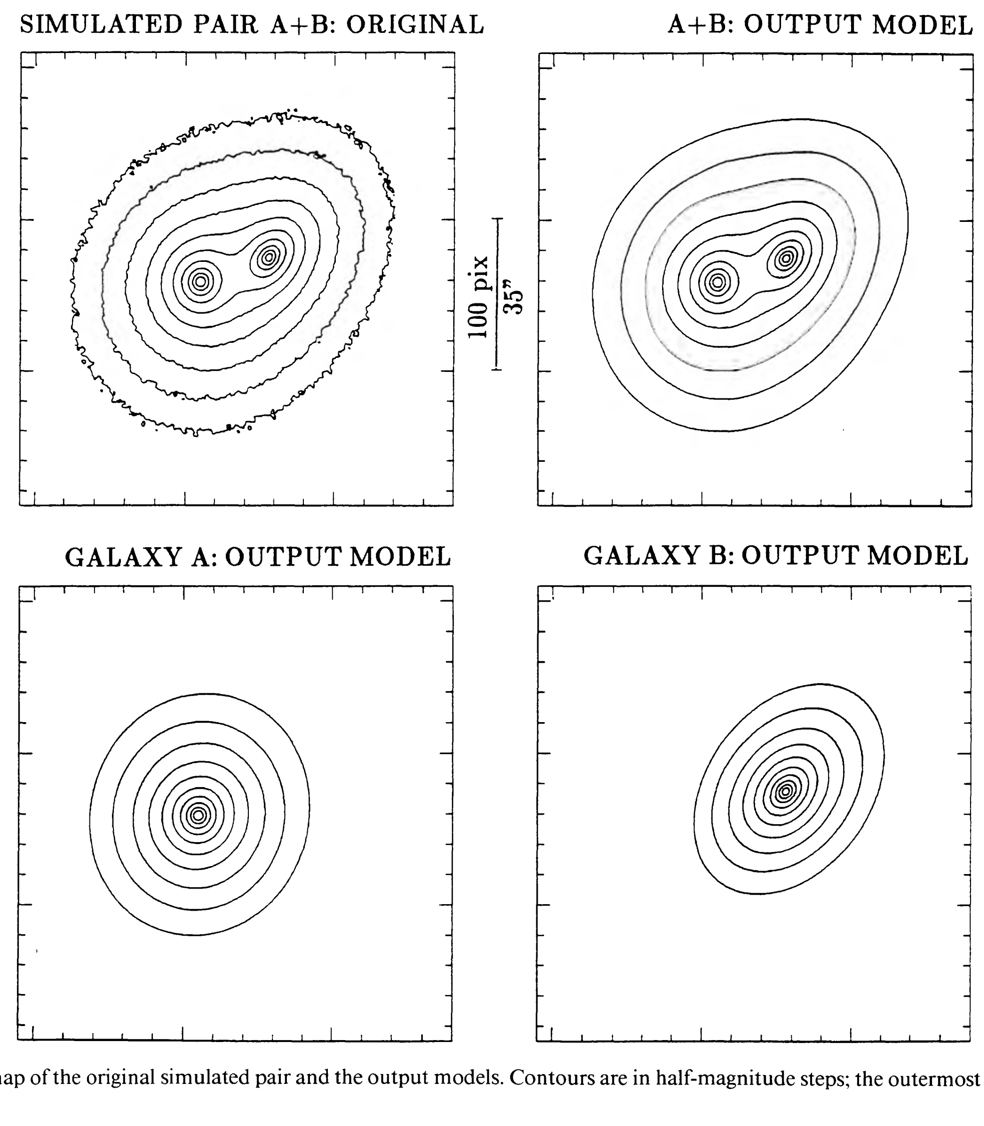

FIG. 3.—Contour map of the original simulated pair and the output models. Contours are in half-magnitude steps; the outermost contour is at 23.3 mag arcsec^{-2}.

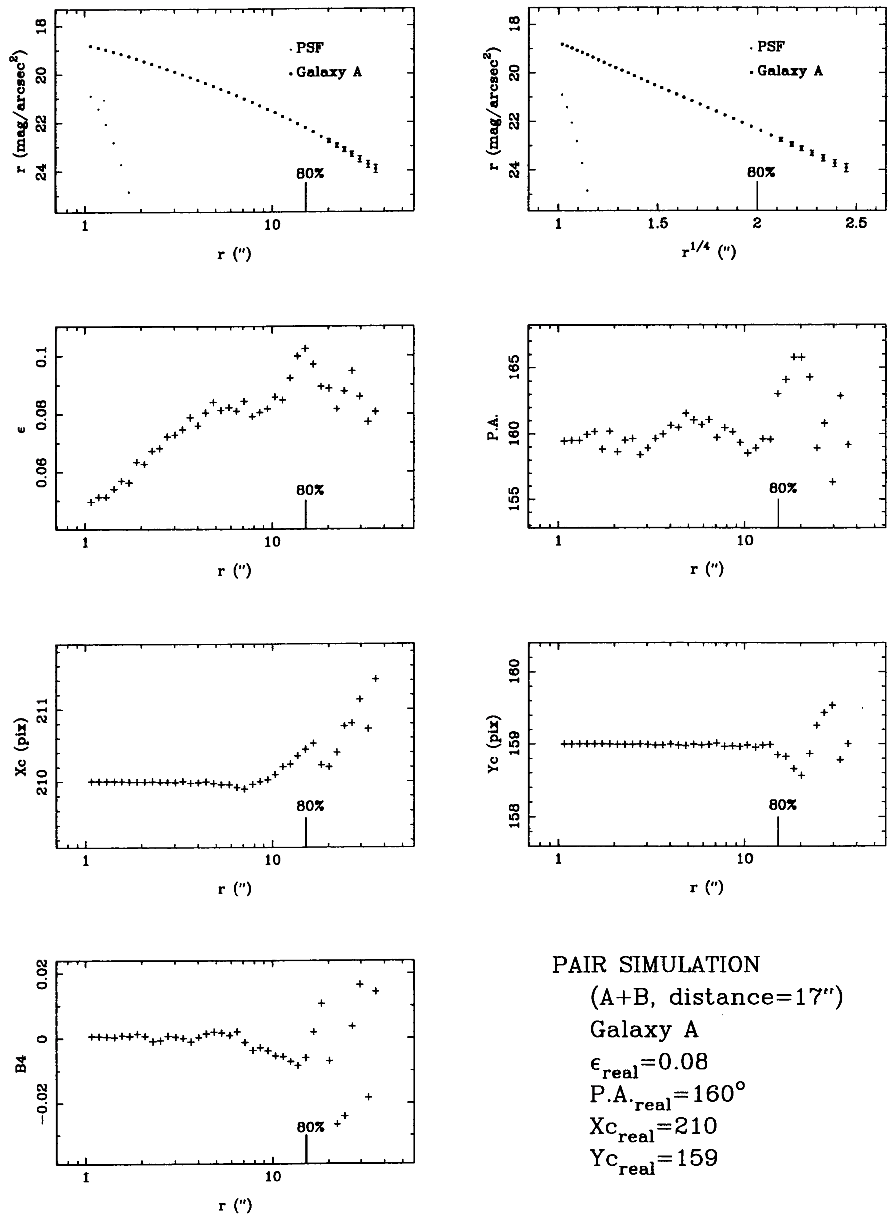

FIG. 4.—Same parameters as in Fig. 2 for the output individual models of the simulated pair

One of these galaxy pairs has been constructed by the superposition of two nearly equal bright elliptical galaxies separated by 17″, i.e., a distance ~0.6 times their effective radius (28″.6 and 28″.2, respectively), whose ellipticities, position angles, and isophote centers were assumed to be constant. After a PSF convolution and noise addition, the system was analyzed in the way discussed in § 3.3. Figure 3 shows the contour plots of the "noisy" original pair and the final model, as well as the resulting individual models. The parameters obtained for the two components of the pair are given in Figure 4 (see § 3.4 for an explanation of these parameters).

Galaxy A surface brightness deviates from the original by ~0.06 mag arcsec^{-2} at a distance equals to its effective radius (28″.6). At that distance, the output ellipticity is ~0.1 instead of 0.08, the deviation of the position angle from the input value is 1°.2, and the isophote center is displaced by 1.1 pixels to the NW from its real position. On average, the magnitude of the output model A deviates from the input by ~0.05 mag arcsec^{-2}, the mean deviations of ellipticity and position angle are 0.025 and 0°.9, respectively, while the mean off-centering of the isophotes is 0.2 pixel.

Similarly, galaxy B output magnitude deviates by ~0.06 mag arcsec^{-2} from the input value at a radius equals to its effective radius (28″.2). At that radius, the deviations of ellipticity and position angle are 0.015 and 2°.2, respectively. The center of the corresponding isophote is displaced by ~2.3 pixels to the NW from its fixed input position. For this galaxy, the mean deviations of the measured magnitude, ellipticity and position angle are 0.06 mag arcsec^{-2}, 0.004 and 0°.9, respectively, while the isophote displacements are, on average, 0.8 pixels with respect to their real position.

González-Serrano & Pérez-Fournon (1991) show a detailed test of this procedure applying it to a simulated pair with a dominant

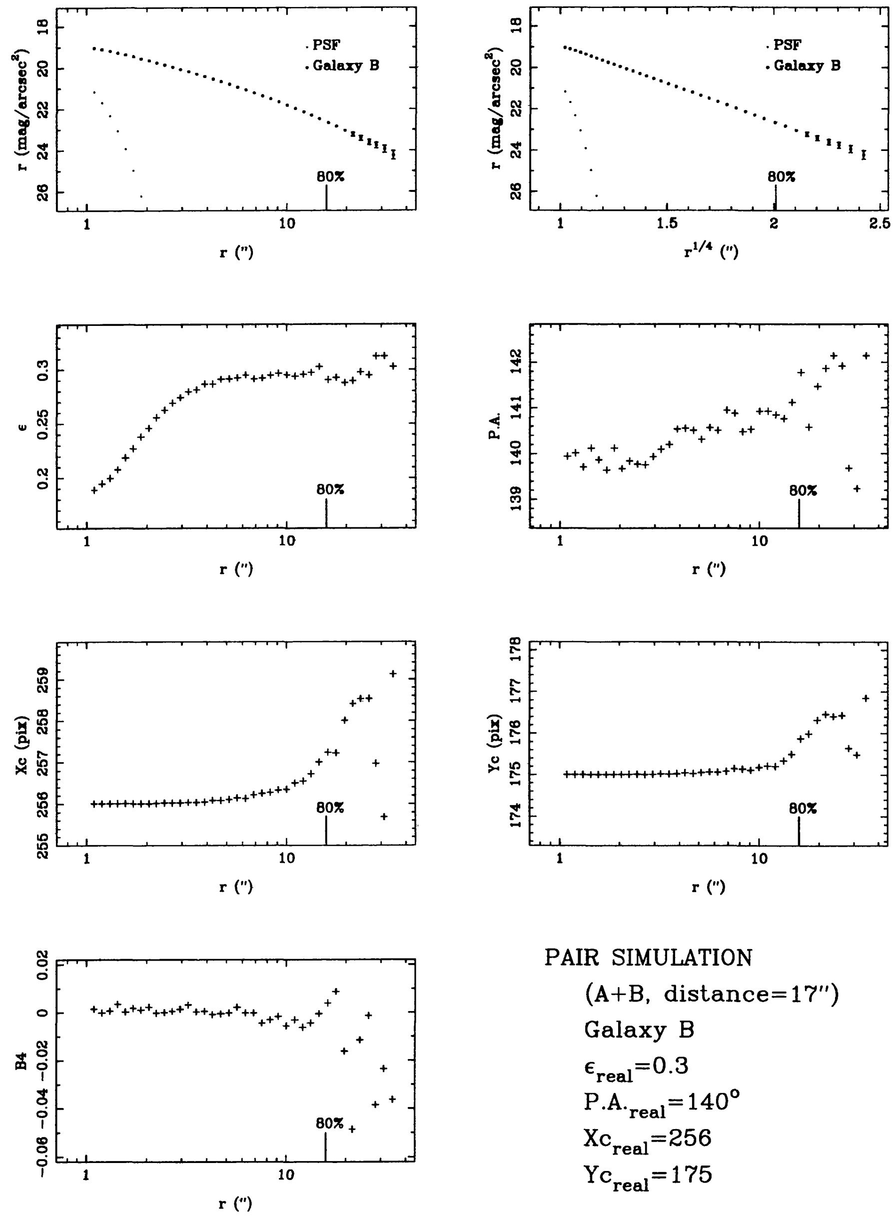

FIG. 4—*Continued*

component separated by 42″ from its secondary companion of relative size $\frac{1}{4}$. Starting with constant parameters in both galaxies and after applying the decomposition algorithm, they find the following results:

In the main component, at a semimajor axis equals to the half-light semi-major axis (42″), the measured magnitude deviates by 0.04 mag arcsec^{-2} from the real value, the ellipticity at that radius is 0.13 instead of 0.1, while the deviations of position angle and isophote center are 4° and 2.8 pixels, respectively.

For the companion, at a semimajor axis equals to the half-light semimajor axis (10″.5), the deviation of the output magnitude is 0.05 mag arcsec^{-2}, the measured ellipticity is 0.11 instead of 0.1, and the deviations of position angle and isophote center are 4° and 0.28 pixels, respectively.

Therefore, these tests show that the iterative decomposition procedure used here is a useful and valid method to analyze pairs (or groups) of galaxies, both in the case of nearly equal bright companions (first test detailed here) and also in the case of one of the companions dominating the light distribution (second test, by González-Serrano & Pérez-Fournon 1991).

REFERENCES

Baum, S. A., Heckman, T. M., Bridle, A., van Breugel, W. H. M., & Miley, G. K. 1988, ApJS, 68, 643

Bender, R., Döbrereiner, S., & Möllenhoff, C. 1988, A&AS, 74, 385

Birkinshaw, M., & Davies, R. L. 1985, ApJ, 291, 32

Borne, K. D., & Colina, L. 1993, ApJ, 416, 157

Bridle, A. H., & Perley, R. A. 1984, ARA&A, 22, 319

Burns, J. O., & Gregory, S. A. 1982, AJ, 87, 1245
Burns, J. O., Hanisch, R. J., White, R. A., Nelson, E. R., Morrisette, K. A., & Moody, J. W. 1987, AJ, 94, 587
Burnstein, D., Davies, R. L., Dressler, A., Faber, S. M., Stone, R. P. S., Lynden-Bell, D., Terlevich, R. J., & Wegner, G. 1987, ApJS, 76, 471
Butcher, H. R., van Breugel, W., & Miley, G. K. 1980, ApJ, 235, 749
Cawson, M. C. 1983, Ph.D. thesis, Univ. Cambridge
Colina, L., & Pérez-Fournon, I. 1990a, ApJ, 348, 45
———. 1990b, ApJS, 72, 41
Ebtener, K., & Balick, B. 1985, AJ, 90, 183
Eilek, J. A., Burns, J. O., O'Dea, C. P., & Owen, F. N. 1984, ApJ, 278, 37
Ekers, R. D., Fanti, R., Lari, C., & Parma, P. 1981, A&A, 101, 194
Forbes, D. A., & Thomson, R. C. 1992, MNRAS, 254, 723
Franx, M., Illingworth, G. D., & Heckman, T. M. 1989, ApJ, 344, 613
Giovannini, G., Feretti, L., & Gregorini, L. 1987, A&AS, 69, 161
González-Serrano, J. I. 1989, Ph.D. thesis, Univ. La Laguna
González-Serrano, J. I., Carballo, R., & Pérez-Fournon, I. 1993, AJ, 105, 1710
González-Serrano, J. I., & Pérez-Fournon, I. 1989, ApJ, 338, L29
———. 1991, A&A, 249, 75
Heckman, T. M., Smith, E. P., Baum, S. A., van Breugel, W. H. M., Miley, G. K., Illingworth, G. D., Bothun, G. D., & Balick, B. 1986, ApJ, 311, 526
Hutchings, J. B. 1987, ApJ, 320, 122
Jedrzejewski, R. I. 1987, MNRAS, 226, 747
Kent, S. M. 1985, PASP, 97, 165
Kormendy, J. 1984, ApJ, 287, 577
Lauer, T. R. 1985, MNRAS, 216, 429
———. 1986, ApJ, 311, 34
———. 1988, ApJ, 325, 49
Longo, L., & de Vaucouleurs, A. 1983, 1985, A General Catalogue of Pholoelectric Magnitudes and Colors in the *UBV* System of 3578 Galaxies Brighter than the 16th *V*-magnitude, Univ. Texas Monograph in Astron. 3 and 3a (Austin: Univ. Texas)
Madejsky, R., Bender, R., & Möllenhoff, C. 1991, A&A, 242, 58
Morganti, R., Fanti, C., Fanti, R., Parma, P., & de Ruiter, H. R. 1987, A&A, 183, 203
Nieto, J. L., McClure, R., Fletcher, J. M., Arnaud, J., Bacon, R., Bender, R., Comte, G., & Poulain, P. 1990, A&A, 235, L17
O'Dea, C. P., & Owen, F. N. 1985, AJ, 90, 927
Owen, F. N., O'Dea, C. P., Inoue, M., & Eilek, J. A. 1985, ApJ, 294, 185
Parma, P., de Ruiter, H. R., Fanti, C., & Fanti, R. 1986, A&AS, 64, 135
Parma, P., Fanti, C., Fanti, R., Morganti, R., & de Ruiter, H. R. 1987, A&A, 181, 244
Peletier, R. F., Davies, R. L., Illingworth, G. D., Davis, L. E., & Cawson, M. 1990, AJ, 100, 4
Pence, W. 1976, ApJ, 203, 39
Pérez-Fournon, I., Colina, L., González-Serrano, J. I., & Biermann, P. L. 1988, ApJ, 329, L81
Perley, R. A., Willis, A. G., & Scott, J. S. 1979, Nature, 281, 437
Riley, J. M., & Pooley, G. G. 1975, MmRAS, 80, 105
Sandage, A. 1973, ApJ, 183, 711
Smith, E. P., & Heckman, T. M. 1989a, ApJ, 341, 658
———. 1989b, ApJS, 69, 365
Sparks, W. B., Wall, J. V., Jorden, P. R., Thorne, D. J., & van Breda, I. 1991, ApJS, 76, 471
Thuan, T. X., & Gunn, J. E. 1976, PASP, 88, 543
van Breugel, W., Filippenko, A. V., Heckman, T. M., & Miley, G. 1985, ApJ, 88, 40